Icarus 450 (2026) 116981

Contents lists available at ScienceDirect

Icarus

journal homepage: www.elsevier.com/locate/icarus

Research Paper

Material dependency in the scaling of low-speed craters under microgravity with implications for small asteroids

Onur Çelik [a,1,*], Ronald-Louis Ballouz [b], Daniel J. Scheeres [c], Yasuhiro Kawakatsu [d]

[a] Faculty of Aerospace Engineering, Delft University of Technology, Delft, 2629 HS, The Netherlands
[b] Applied Physics Laboratory, The Johns Hopkins University, Laurel, MD 20723, Maryland, United States
[c] Ann and H.J. Smead Aerospace Engineering Sciences, University of Colorado Boulder, CO 80903, Colorado, United States
[d] Department of Space Systems, Japan Aerospace Exploration Agency (JAXA), Sagamihara, 252-5210, Kanagawa, Japan

ARTICLE INFO

Keywords:
Solar system
Asteroids
Impact crater
Scaling relationships
Discrete element method (DEM)

ABSTRACT

Small body surfaces are covered by granular material of varying particle sizes and depths. This material is observed to be easily mobilised from the surface through natural processes or spacecraft interaction. The material can escape or re-impact to the surface as a result of this process. The latter may be considered as a low-speed cratering activity under microgravity. In this paper, a set of simulations of normal impacts at 5–10 cm/s under 9.81×10^{-5} m/s^2 is presented with gravel-type realistic material properties. The simulated craters are investigated for their qualitative impact outcomes, as well as quantitatively for the coefficient of restitution and crater and ejecta scaling properties. The results are compared with the results of impacts in glass beads type materials from authors' previous work under the same conditions and wider literature experimental and observational literature. It was shown that most impacts result in a rebound with non-negligible coefficient of restitution values. The crater sizes are smaller compared to those in glass beads material and follows the crater scaling relationships across different impact energies with a μ coefficient of 0.55. Ejection is shown to continue beyond the final size with a significant quantity of material mobilised at speed below escape speed under the selected gravity level. The depth-to-diameter ratio of the craters is within the range of small craters of asteroid Bennu, with qualitative impact outcomes displaying similarities with those found in this paper. These results suggest a possible low-speed impact and secondary cratering activity in small bodies as a result of natural and artificial particle ejection events, such as in the case of Bennu and Didymos.

1. Introduction

Space missions thus far have shown that asteroids and comets are covered with loose granular material of variable depths called regolith. This regolith is observed to mobilise easily, either by natural processes or during the surface operations of a spacecraft. An example of the former is high-energy impacts, which often result in large-scale outcomes which may be observed even by terrestrial platforms such as telescopes, similar to planetary defense mission DART's kinetic impact on Didymos (Daly et al., 2023). However, another class of impacts may also be defined, hereafter called low-speed impacts, which may be secondary, low-energy impacts resulting from high-energy impacts (Nakamura et al., 2008), seismic shaking (Tancredi et al., 2012) or due to material ejection in small bodies, such as the particle ejection and re-impact events recently observed asteroid Bennu (Lauretta et al., 2019). Bennu's material ejection is attributed to a number of different possible mechanisms (Chesley et al., 2020; Bottke et al., 2020) and, as observed, particles with low energy (i.e., below the necessary escape energy), would re-impact the surface or even ricochet (Pelgrift et al., 2020). Low-speed impacts in this context can then be approximately defined as impacts at or below speeds of the order of escape speed of small asteroids, which is typically around a few tens of cm/s (for example, ~30 cm/s for Bennu). Impacts at this energy level would only be observable during close observations and would contribute to a more subtle but potentially gradual physical and dynamical evolution of a small body (Scheeres et al., 2019). In addition, regolith mobility may also be possible due to spacecraft-surface interaction, namely through ballistic landings of small landers (Çelik and Sanchez, 2017; Çelik et al., 2019a), through the sampling operations of spacecraft (Tsuda et al.,

* Corresponding author.
E-mail addresses: o.celik-1@tudelft.nl (O. Çelik), ronald.ballouz@jhuapl.edu (R.-L. Ballouz), scheeres@colorado.edu (D.J. Scheeres), kawakatsu@jaxa.jp (Y. Kawakatsu).

[1] A part of this study was performed when Onur Çelik was a Ph.D. candidate at the Graduate University for Advanced Studies, SOKENDAI, Sagamihara, 252-5210, Japan and a visiting scholar at University of Colorado Boulder CO 80903, USA

https://doi.org/10.1016/j.icarus.2026.116981
Received 6 August 2025; Received in revised form 28 January 2026; Accepted 28 January 2026
Available online 29 January 2026

2020) or through dedicated impact experiments (Arakawa et al., 2020). These artificial impacts in small bodies may also be viewed from a low-speed impact perspective, from which the outcomes of the impacts may help understand the surface of a small body (particularly in terms of its strength) (Murdoch et al., 2021; Ballouz et al., 2021; Walsh et al., 2022) and help build confidence in landing operations (Çelik et al., 2017, 2019b).

The low-speed impacts discussed above can be considered as a form of impact cratering in microgravity. Indeed, the dimple-like structures in Itokawa's regolith-covered plains have boulders within the crater bowl with sizes are approximately between 25% and 50% of the crater size and could be associated with low-speed impacts (Kiuchi et al., 2019). As an example, the impact of the largest ejected particles of Bennu (~10 cm (Lauretta et al., 2019; Pelgrift et al., 2020)) at 25 cm/s could create a crater of nearly 70 cm in diameter (Çelik et al., 2022). Moreover, recent observational results from Bennu's small craters (as small as ~ 1 m) show nearby boulders as large as half the size of the crater (Daly et al., 2022), which may be associated with low-speed impacts. Similarly, the observations and simulations of the ejecta of DART impact suggests that there may be a secondary impact activity, which are more likely to occur below the escape speed of asteroid Didymos (Kareta et al., 2023). Some of the re-impacting particles have likely created secondary craters and even potentially rebounded off the surface to be temporarily captured in the binary system (Kareta et al., 2023; Moreno et al., 2024). The latter rebound behaviour is also observed in experimental and numerical studies of low-speed impacts (Katsuragi and Blum, 2017; Brisset et al., 2018, 2020; Çelik et al., 2022). Given the low cohesive strength found in these asteroids (Walsh et al., 2022), the source of strength primarily comes from the frictional interaction between the particles. Therefore, simulating low-speed impacts with realistic material properties is paramount to understanding these impact outcomes.

It is, however, challenging to test this regime in the Earth-based platforms. In impacts at a few tens of cm/s under terrestrial gravity, gravitational overburden pressure dominates over frictional effects leading to surface strengths that are orders of magnitude larger than those encountered on the surfaces of small asteroids. Note the SCI experiments as an example, where material ejection is observed for minutes after the impact of 2 km/s projectile (Arakawa et al., 2020). Terrestrial artificial low-gravity platforms, such as the International Space Station, parabolic flights, drop towers or air-bearing platforms either lack the necessary low-gravity level and/or duration or they present other challenges (e.g., accessibility, handling of granular material in low gravity, etc.) that make low-speed cratering experiments at this regime very challenging (Colwell and Taylor, 1999; Gautier et al., 2020; Van wal et al., 2021). Such challenges often limit the low-speed cratering studies to post-impact crater size measurements only (Boudet et al., 2006; De Vet and De Bruyn, 2007; Kiuchi et al., 2019; Takizawa and Katsuragi, 2020), indirect deductions of ejecta speeds (Deboeuf et al., 2009) or rather qualitative analysis of ejected mass (Brisset et al., 2018). Nevertheless, combined with other impact experiment studies at 10-to-100 m/s range in both terrestrial and low-gravity environments (Cintala et al., 1989; Yamamoto et al., 2006; Tsujido et al., 2015), the validity of crater scaling relationships (Housen et al., 1983) are confirmed in lower speed impacts.

Discrete element method (DEM) simulations, on the other hand, provide a particle-level quantitative framework to test low-speed impacts in this regime in virtually any gravitational environment (Wada et al., 2006; Sánchez and Scheeres, 2011; Maurel et al., 2018; Thuillet et al., 2018; Çelik et al., 2019a; Ballouz et al., 2021; Çelik et al., 2022). Each particle's state can be recorded, allowing opportunities for more detailed investigations without the measurement limitations of experimental platforms. Its deterministic nature means that the simulations can be carried out only once, thus reducing the number of tests necessary. To that end, Çelik et al. (2022) recently used DEM simulations to extend the applicability of crater-scaling relationships in gravity regime, including ejecta velocity (speed and angle), ejected mass and crater formation time, to impacts at 5–50 cm/s in local vertical under microgravity similar to small asteroids such as Ryugu and Bennu, via a particle-level post-processing framework. The authors found the scaling exponent μ, signifying the mode of coupling between impactor and target, as $\mu = 0.56$, implying an impactor energy-driven cratering (Çelik et al., 2022). This value is higher than terrestrially observed ~0.4 (Housen and Holsapple, 2011), with a very weak relationship to impactor density (Çelik et al., 2022). The exaggerated cratering behaviour is attributed to emulated smooth glass-bead material used in the simulations (Çelik et al., 2022; Wada et al., 2006; Housen and Holsapple, 2011) and argued that more frictional material properties would result in more realistic cratering (Çelik et al., 2022).

In this paper, therefore, a new set of impact simulations is presented with gravel-like material to test low-speed cratering in small solar system bodies in a more realistic manner. The simulations are performed with soft-sphere DEM (SSDEM) code `pkdgrav` (Schwartz et al., 2012) where the impacts are parallel to the surface normal and at 5–10 cm/s under 9.81×10^{-5} or $10^{-5}g$ (where g is the Earth's gravitational acceleration). A quantitative analysis on the coefficient of restitution is first presented as the rebound behaviour is the dominant post-impact outcome. Then, the results of crater size scaling are analysed alongside the properties such as the depth-to-diameter ratio, ejecta properties, including the number and the mass of the particles ejected. A comparative approach is taken throughout the paper and the results are compared against the simulations with glass-beads materials (Çelik et al., 2022) and other experimental and observational results. The implications of the results are also discussed.

The paper is structured as follows: In the next section, a summary of the crater scaling relationships will be presented. After summarising the simulation conditions in Section 3, the results will be discussed in Section 4, alongside a comparison with glass beads like material. A comparison with the existing literature is provided in Section 5 before a discussion and conclusions in Sections 6 and 7, respectively.

2. The crater-scaling relationships

The crater scaling relationships are initially derived for high-energy impacts where thermo-mechanical processes such as melting, vaporising and breaking occur (Melosh, 1989). The physics of such complex processes can be simulated by sophisticated hydrocode simulations, but if this process is bypassed, the properties of the resulting craters can be connected to the impact, impactor, and surface properties through the crater-scaling relationships (Holsapple and Schmidt, 1982; Housen et al., 1983; Housen and Holsapple, 2011). These relationships rely on dimensional analysis with π-theorem (Buckingham, 1914) and express crater or ejecta properties in the form of power-law scaling in relation to impact speed, impactor size and density and macro surface properties gravity, density and strength to avoid granular level complexity (Fig. 1) (Holsapple and Schmidt, 1982; Housen et al., 1983; Housen and Holsapple, 2011). This section will present the fundamental relationships for crater sizes and ejecta properties.

2.1. Scaling of crater sizes

The main assumption of the relationships is that a few key macro parameters can be used to express a functional relationships between them and a crater parameter, such as its volume, V:

$$V = f(a, \delta, U, \rho, Y, g) \tag{1}$$

The definitions of the parameters will be referenced frequently in the remaining of the paper, hence Table 1 is used to describe each of them alongside their units.

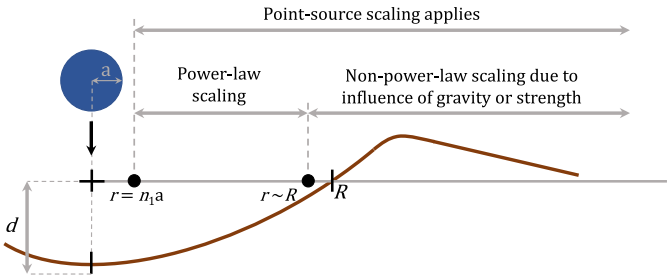

Fig. 1. Profile of a crater and power-law scaling. *Source:* Adapted from Housen and Holsapple (2011), Çelik et al. (2022).

Table 1
Glossary of crater-scaling relationships.

Symbol	Definition
V	Crater volume [m^3]
R	Crater radius [m]
d	Crater depth [m]
a	Impactor radius [m]
δ	Impactor density [kg/m^3]
m	Impactor mass [kg]
U	Impact velocity [m/s]
ρ	Target bulk density [kg/m^3]
Y	Target strength [Pa]
g	Gravitational acceleration [m/s^2]
r	Ejecta launch position on the target surface [m]

By using the units of mass, length and time, the number of parameters can be reduced to 4 from 7, which can be expressed as individual π parameters:

$$\pi_V = V\frac{\rho}{m} \tag{2a}$$

$$\pi_2 = \frac{ga}{U^2} \tag{2b}$$

$$\pi_3 = \frac{Y}{\rho U^2} \tag{2c}$$

$$\pi_4 = \frac{\rho}{\delta} \tag{2d}$$

where π_V is normalised volume, π_2 is inverse Froude number or gravity scaling parameter, π_3 is nondimensional strength and π_4 is target-to-impactor density ratio. These four parameters can be combined to describe the functional relationship:

$$\pi_V = K_V \pi_2^{-\alpha}\pi_3^{-\beta}\pi_4^{-\gamma} \tag{3}$$

where K_V, α, β, γ are empirical constants (Holsapple and Schmidt, 1982). Making use of a coupling parameter such as $C = aU^{\mu}\delta^{\nu}$ and rewriting Eq. (1) yields (Schmidt and Housen, 1987):

$$V = f(C, \rho, Y, g) \tag{4}$$

Here C is a parameter to describe the concept "late-stage equivalence," which, for high-energy cratering, means that cratering process far from the impact point is not affected by the impactor dimensions, and justifies the use of a point-mass impactor (Schmidt and Housen, 1987). It is not yet clear whether this can be applied to such low-energy impact craters discussed here, but previous studies successfully demonstrated the applicability of the crater scaling relationships for low-speed impacts (Çelik et al., 2022; Takizawa and Katsuragi, 2020) hence, the validity is assumed in this study. Dimensional analysis can be applied again to Eq. (4) to finally find the relationship:

$$\pi_V = K_1\left[\pi_2\pi_4^{\frac{6\nu-2-\mu}{3\mu}} + \left(K_2\pi_3\pi_4^{\frac{6\nu-2}{3\mu}}\right)^{\frac{2+\mu}{2}}\right]^{\frac{-3\mu}{2+\mu}} \tag{5}$$

where K_1, μ and ν are two empirical constants (Housen et al., 1983). μ describes a mode of coupling between the impactor and target and its values are constrained between 1/3 and 2/3, where the lower end signifies dependency on impactor momentum whereas the higher end signifies dependency on impactor energy (Housen et al., 1983). ν on the other hand describes a density dependency of cratering, whose value is constrained to ~0.4 (density independence) for high-energy cratering in dry sand, but the literature presents values as high as 0.57 (Tsujido et al., 2015). Eq. (5) also describes two regimes of cratering (Holsapple and Schmidt, 1982; Housen et al., 1983). If the first term in the square bracket is significantly larger than the second, the crater is said to form in a gravity regime, whereas in the opposite situation it is said to form in a strength regime (Holsapple and Schmidt, 1982). This study does not consider cohesive strength in the target material. The strength arising due to frictional interaction within the granular materials is not considered part of the material structure and is not included in the Y term in Eq. (5) (Holsapple and Schmidt, 1982). The remaining derivation will therefore omit the second term in the square bracket, i.e., $\left(K_2\pi_3\pi_4^{\frac{6\nu-2}{3\mu}}\right)^{\frac{2+\mu}{2}}$. Substituting π values into Eq. (5) would then yield (Holsapple, 1993):

$$V = K_1\left(\frac{m}{\rho}\right)\left[\left(\frac{ga}{U^2}\right)\left(\frac{\rho}{\delta}\right)^{\frac{6\nu-2-\mu}{3\mu}}\right]^{\frac{-3\mu}{2+\mu}} \tag{6}$$

It is often easier to measure a crater's radius or diameter than its volume. Craters occur after an impact in local normal would typically take the form of a circular paraboloid (Melosh, 1989), whose volume can be written as:

$$V = \frac{1}{2}\pi R^2 d \tag{7}$$

where d denotes the depth of the paraboloid, specifically for the craters in this paper. Assuming $R \sim V^{1/3}$ and substituting in Eq. (6) yield:

$$R = K_R\left(\frac{m}{\rho}\right)^{\frac{1}{3}}\left[\left(\frac{ga}{U^2}\right)\left(\frac{\rho}{\delta}\right)^{\frac{6\nu-2-\mu}{3\mu}}\right]^{\frac{-\mu}{2+\mu}} \tag{8}$$

Finally, a normalised crater size can be defined such that:

$$\pi_R = R\left(\frac{\rho}{m}\right)^{1/3} \tag{9}$$

π_R can then be used as a term of equivalency to evaluate crater size for a given impact, impactor, and target properties.

2.2. Scaling of ejection properties

The magnitude of the velocity of the ejected material can also be scaled similarly to the crater size as a function of the launch position from the impact point on the target surface, r (Housen and Holsapple, 2011):

$$v(r) = C_1\sqrt{gR}\left(\frac{r}{R}\right)^{-1/\mu} \tag{10}$$

where C_1 is an empirical constant. Eq. (10) is another power law scaling, meaning that the ejecta speed may be expected to be much higher close to the impact point and rapidly decreases towards the crater radius. One potential drawback of this expression is that v tends to zero at the crater radius, but recent studies show that the ejection may indeed extend beyond the crater radius for low-speed impacts (Çelik et al., 2022; Neiderbach et al., 2023), which will also be discussed in this paper.

Another aspect of the ejected material is its quantity, which can be found as a function of ejecta speed (Housen and Holsapple, 2011):

$$M(>v) = C_2\rho R^3\left(\frac{v}{\sqrt{gR}}\right)^{-3\mu} \tag{11}$$

where $M(>v)$ describes the total mass ejected faster than speed v (Housen and Holsapple, 2011). Again, C_2 is another empirical constant. Because of the intrinsic position dependency of $v(r)$, i.e., $M(>v(r))$, Eq. (11) may also be considered as the total mass ejected within

Table 2
Summary of SSDEM material parameters (Ballouz et al., 2015). k_n value is calculated from Schwartz et al. (2012).

Parameters	Glass beads (GB) (Çelik et al., 2022)	Gravel (GR)
ϵ_n	0.95	0.55
ϵ_t	1.0	0.55
μ_s	0.43	1.31
μ_r	0.1	3.00
k_n	75.25 kg/s^2	

a given radial distance. It is worth noting that equivalent expressions of Eqs. (10) and (11) may be found as a function of impactor properties (Housen and Holsapple, 2011). The applicability of these scaling relationships is described from some $r = n_1 a$ to $r \sim R$ (Housen and Holsapple, 2011). Even though the exact range applicability is unclear, it is generally assumed that $n_1 \approx 1.2$ (Housen and Holsapple, 2011), as also shown in Fig. 1. This will not be tested specifically in this paper and will be shown intrinsically while presenting scaling relationships after the simulations. Next, the details of these simulations are presented.

3. Discrete element method (DEM) simulations

The simulations in this paper are performed with a granular mechanics code `pkdgrav`. `pkdgrav` handles the interactions between the particles via the soft-sphere discrete element method (SSDEM) (Schwartz et al., 2012). The multiple contacts and frictional interactions between particles are simulated by springs and a set of coefficients of normal (ϵ_n) and tangential (ϵ_t) restitution, Coulomb (μ_s), rolling (μ_r) and twisting (μ_{tw}) frictions (Schwartz et al., 2012). The twisting friction is not used in the simulations presented here, but expresses the energy dissipation between particles as they rotate around the normal of their contact region, i.e. "grind" each other (Schwartz et al., 2012). In addition to material parameters the coefficients of rolling and twisting frictions, `pkdgrav` also has the capability to account for the non-sphericity of particles through a user-defined, statistical real shape parameter, β, which defines the contact width of interparticle penetration, scales rolling and twisting frictions and can be chosen by comparing the internal friction angle of the granular assembly to the target granular material (Jiang et al., 2005; Zhang et al., 2017). More details about `pkdgrav` and the material parameters can be found in Schwartz et al. (2012), Zhang et al. (2017).

`pkdgrav` is extensively tested against real world materials and a range of parameters are identified through angle-of-repose, impact and simple avalanche experiments for glass-beads and gravel type materials (Richardson et al., 2012; Yu et al., 2014; Ballouz et al., 2015, 2021; Schwartz et al., 2014). The spring coefficient, k_n, represents the coefficient of a normal spring, used to control the amount of interparticle penetration, typically at approximately 1% (Schwartz et al., 2012). k_n is set in relation to the maximum expected impact speed between particles (Schwartz et al., 2012), which is controlled by the free-fall speed of particles during the preparation stage of the simulated target material. In this study, gravel-like material parameters are used for the impact simulations, as presented in Ballouz et al. (2015), and also shown in Table 2 below.

Note also the glass-beads-like (GB) material parameters in Table 2, which the authors previously used to perform low-speed impact simulations under the gravitational acceleration 9.81×10^{-5} m/s^2 (Çelik et al., 2022). The gravel-like parameters (GR) used in this paper are more frictional with lower coefficients of restitution compared to the GB parameters. Higher friction between particles provides additional strength to the surface, which leads to higher angle of repose values (Yu et al., 2014; Housen and Holsapple, 2011).

The granular bed used in the impact simulations is generated by first setting a cloud of 40000 2 cm-diameter monodisperse spherical particles. The particles are smooth spheres but angularity is introduced

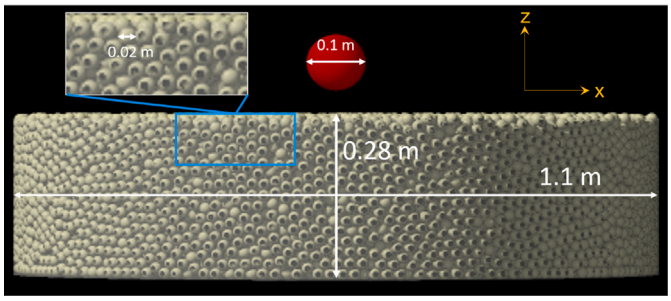

Fig. 2. Initial setup of `pkdgrav`.

with the β parameter. The particles are randomly located within a cylindrical diameter of 1.1 m initially, i.e. the same as the diameter of the granular bed. The particle sizes are not varied to remove any particle-size dependencies in the impact outcomes. The cloud of particles are released for a free fall into the container of aforementioned diameter and 0.28 m of depth. A post-processing code is used to remove any particles that are higher than this depth at the end of the settling, such that a flat surface is created. The final number of particles in the container is equal to 38723. Fig. 2 shows the appearance of this final granular bed after the post-processing.

The density of particles, ρ_p, is selected to be 1600 kg/m^3. No specific material is targeted in this study, but the selected density is an estimated value for porous carbonaceous materials (Kuzmin et al., 2003). The porosity value in the final settled granular bed is equal to 39.04%, resulting in a bulk density $\rho = 975.4$ kg/m^3. This relatively lower bulk density is close to the density values measured in the upper layers of asteroid Bennu (Walsh et al., 2022), thus it may be representative of such a case.

Finally, the impacts on this granular bed are performed with a 10 cm-diameter spherical impactor. `pkdgrav` also allows simulations with other simple geometric shapes (Ballouz, 2017) such as cylinders and rectangular, which are used in ballistic landing simulations previously (Maurel et al., 2018; Çelik et al., 2019a). The impactor density values are 100, 260, 347, 520, and 1910 kg/m^3. Such a range of densities is included to explore a wide variety of impact outcomes, but recent observations suggest that boulders on the floors of small craters (<20 m) on Ryugu may be very porous (>70%) (Sakatani et al., 2021), such that low-density boulders may exist. Moreover, many lander spacecraft have relatively low densities. For example, Philae lander onboard Rosetta mission is approximately 100 kg with dimensions 1 m x 1 m x 0.8 m in all directions (Biele et al., 2015). With the assumption of a cube shape, the lander density becomes 125 kg/m^3. Therefore the selected density range covers both natural and human-made objects. Finally, the selected densities for the particles and impactor result in a 6.7 g particle and an impactor mass between 52 g to 1000 g, approximately between 8 to 150 times the particle mass.

The impacts are performed in the container's local vertical parallel to the gravity vector. In the container frame, as shown in Fig. 2, the z direction is defined as the direction opposite to the gravity vector in a left-handed reference frame, the y-axis points the out-of-paper (of the *viewer*) direction while the x-axis completing the triad. Two impact speeds, 5 cm/s and 10 cm/s are considered, which are among the most common ejection speeds observed in Bennu (Pelgrift et al., 2020), representative of the touchdown speeds of OSIRIS-REx (Lauretta and OSIRIS-REx TAG Team, 2021) and Hayabusa2 (Tsuda et al., 2020), as well as, close to first and within the secondary impact speeds of ballistic landers such as MASCOT (Scholten et al., 2019). The gravitational acceleration is 9.81×10^{-5} m/s^2, similar to Bennu and Ryugu (Scheeres et al., 2019; Kitazato et al., 2019). Table 3 summarises the parameter space covered in this paper.

Table 3
Covered parameter space during simulations.

Parameter	Value
a [m]	0.05
δ [kg/m^3]	100, 260, 347, 520, 1910
U [m/s]	0.05, 0.1
ρ [kg/m^3]	975.36
ρ_p [kg/m^3]	1600
r_p [m]	0.01
ϕ [%]	39.04
g [m/s^2]	9.81 × 10^{-5}

The selected diameters of the impactor and particles result in an impactor-to-particle size ratio of 5, which is smaller than the ratios in terrestrial high-speed impact experiments, but is within the range where it is considered to be not influencing the crater-scaling outcome as discussed by Housen and Holsapple (2011) for high-energy impacts. This means that, even though the crater size or ejection speed is different between different impactor-to-particle size ratios, the scaled outcome would be on the same empirical relationship defined primarily by μ, K_1 and ν. The interpretation of the effect of impactor-to-particle ratio by Housen and Holsapple (2011) is also confirmed by Çelik et al. (2022) for low-speed impacts and suggested that the ratio may even be lower at 3, at least in the impact regime considered here. Related to this point, the container-to-impactor size ratio is equal to 11, well above the minimum ratio (i.e., 5) below which the container size is considered to affect impact outcomes (Seguin et al., 2008). The container walls are assigned a coefficient of restitution value of 0.1 such that the reflection from the container walls are minimised.

The simulations were stopped after approximately 6 min, within which particle speeds are found to be below 0.1 mm/s. An integration time step is 0.7 mm/s and an output step of 2500 is selected, such that an output file is generated approximately every 1.8 s of the impact process. General features of low-speed cratering and its ejection process are captured for the purposes of this study by the selection of this data-output frequency. The obtained data is then post-processed to extract the information related to cratering, including crater radius, ejection velocity and ejected mass according to the post-processing procedure described in Çelik et al. (2022). The results of the analysis is presented in the next section.

4. Low-speed cratering with gravel-like material

4.1. Qualitative impact outcomes

Some generic properties of the craters will be discussed first. As such, the qualitative impact outcomes are presented in Fig. 3.

Among all the impactor density, δ, values, only those with $\delta = 1910$ kg/m^3 (or $m = 1$ kg) are submerged while others rebounded off the surface after a brief penetration and mobilising some material from the surface. Rebound behaviour of spherical impactors in local vertical impacts is a relatively unobserved phenomenon in dry sand, even though it was previously reported in cohesive granular material for low-speed impacts under low gravity (Brisset et al., 2018) and under terrestrial gravity (Katsuragi and Blum, 2017). For non-spherical impactors, it may occur depending on the impactor attitude and rotation at impact for the low-speed impact regime under low gravity (Maurel et al., 2018; Çelik et al., 2019a). However, it is a much more frequent occurrence in oblique impacts under both terrestrial and low-gravity environments for both low- and high-speed impacts (Gault and Wedekind, 1978; Takizawa and Katsuragi, 2020; Wright et al., 2020b; Chesley et al., 2020; Suo et al., 2024).

These impacts also result in a variety of qualitative impact outcomes. These qualitative impact outcomes may be of additional interest to relate a boulder to a nearby crater in small body surfaces. Four of those are depicted in Fig. 4.

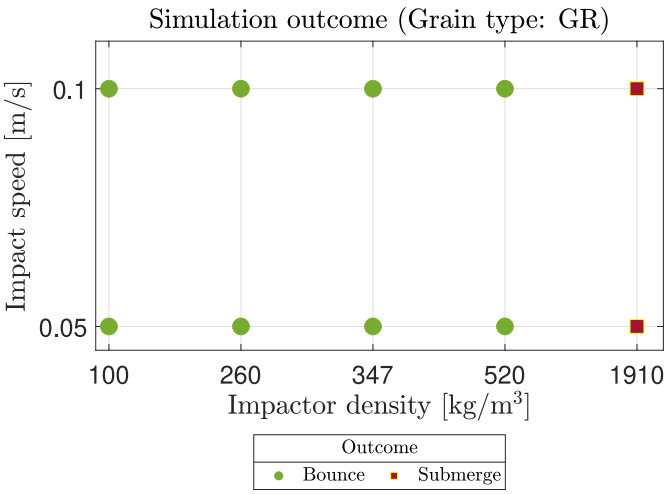

Fig. 3. Qualitative simulation outcomes with gravel-like (GR) material.

In the figure, the red circle denotes the final location of the impactors in a quasi-two-dimensional view, where the depth is only two-particle length, that is why the upper left panel appears as if the impactor is filled with particles. The first case in the upper left panel is an example of a submerged impactor, which steers towards the $+x$ direction after the impact instead of penetrating in the -z direction, and stays in the crater wall. In the second case at the upper left panel, the impactor instead rebounds from the surface and disappears from the view. In the bottom two case, the outcomes appear similar, but the process prior to that is different. In the case of the lower left panel, the impactor initially rebounds and follows a projectile motion before coming to stop. Instead in the case of the lower right panel, the impact rebounds off the surface and makes a very brief projectile motion before it starts rolling in the $+x$ direction and comes to a stop. This rolling behaviour is also discussed in Brisset et al. (2020), and they argued that it may be a result of the impactor-to-particle size ratio. A smaller ratio would correspond to a smaller interaction area between the impactor and the surface, whereas in the opposite case an almost continuous interaction surface is created. This may result in a motion determined by the interaction between a few grains and the impactor. Additionally, in the simulations here, low restitution coefficients, and high static and rolling friction between particles could further enhance this behaviour, both in the rebound and submerge cases, such as in the outcome in the upper left panel in Fig. 4.

Fig. 4 also shows the crater profiles. In the submerging case in the upper left panel, a prominent crater structure is apparent, with raised rims and a bowl shape. Despite the burial of the impactor in one of the crater walls, the shape is relatively symmetric around the z-axis. In the rebound cases, it can be observed that craters become shallower with lower rims, although the bowl shape is still apparent. In the next subsection, the impact outcome will be investigated from a more quantitative perspective by considering the coefficient of restitution.

4.2. The coefficient of restitution

As the rebound behaviour is the dominant post-impact outcome in these impacts, the coefficient of restitution is of interest. In this paper, it is defined as the ratios of outgoing and incoming velocity magnitudes such that:

$$\epsilon = \frac{v^+}{v^-} \tag{12}$$

where ϵ denotes the coefficient of restitution, whereas v^+ and v^- are outgoing and incoming velocity magnitudes, respectively. This formulation is adopted to account for the post-impact motion of the

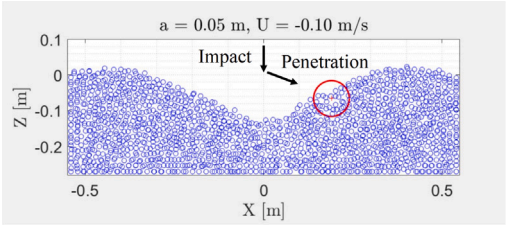

(a) Example outcome #1 (U = 10 cm/s, δ = 1920 kg/m^3)

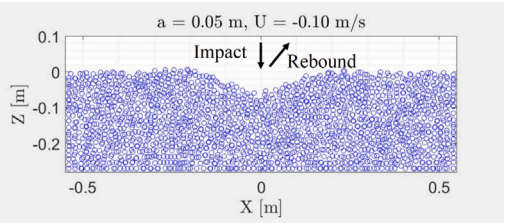

(b) Example outcome #2 (U = 10 cm/s, δ = 260 kg/m^3)

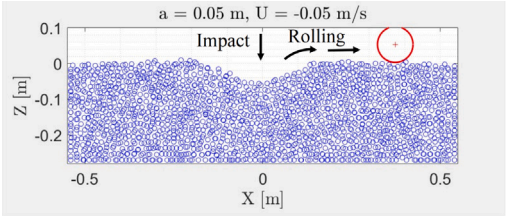

(c) Example outcome #3 (U = 5 cm/s, δ = 520 kg/m^3)

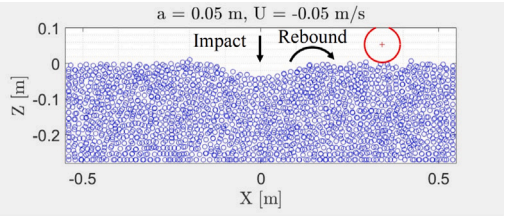

(d) Example outcome #4 (U = 5 cm/s, δ = 347 kg/m^3)

Fig. 4. Various qualitative impact outcomes found in this study.

Table 4
The coefficient of restitution values in each impact simulation with gravel-type materials.

Density [kg/m^3]	Coefficient of restitution, ϵ [-]	
	U = 5 cm/s	U = 10 cm/s
100	0.278	0.256
260	0.158	0.204
347	0.121	0.194
520	0.124	0.175

impactor, which is not necessarily in the local vertical direction due to the interaction with the granular surface. ϵ is then calculated at the first instance where the impactor's z component of the velocity vector is positive, which is not the same point in all impact cases due to the discrete data collection. The ϵ values are presented in Table 4.

It is worth noting that the impactor is given a coefficient of restitution value of 0.6 in the simulations to consider real-world cases such as landers. Hence the calculated values in Table 4 may be higher or lower depending on the coefficient of restitution of the impactor material.

In general, ϵ decreases with increasing density values. The highest ϵ is equal to 0.278 and calculated for the lowest impact speed and density. ϵ decreases with each subsequent density value for both cases, though there is a small increase at δ = 520 kg/m^3 case of 5 cm/s impact case. This may be due to the discrete data collection strategy. Except for the lowest density case, all impacts with 10 cm/s speed have higher ϵ. In the GR-like material, increased friction between the grains likely provides some additional resistance to the material penetration.

4.3. Crater morphology and ejecta properties

The post-processing procedure described in Çelik et al. (2022) is applied to the raw impact data, and the cratering results in Table 5 are obtained.

The values in Table 5 can now be used to investigate various crater scaling relationships. Consider the following expression from π-scaling relations provided in Section 2:

$$R\left(\frac{\rho}{m}\right)^{\frac{1}{3}} = K_R\left(\frac{ga}{U^2}\right)^{-\frac{\mu}{2+\mu}}\left(\frac{\rho}{\delta}\right)^{\frac{6\nu-2-\mu}{3(2+\mu)}} \tag{13}$$

In π-scaling terms, the equation would take the following form:

$$\pi_R = K_R\pi_2^{-\alpha}\pi_4^{-\gamma} \tag{14}$$

Table 5
Tabulated simulation conditions and outcomes. All simulations under 9.80665×10^{-5} m/s^2 ($1\times10^{-5}g$). The radius of all impactors is 0.05 m. Outcome: Qualitative simulation output. S: Submerge. B: Rebound/Bounce.

#	U [m/s]	δ [m^3]	R [m]	d [m]	Outcome
1	0.05	100	0.0884	0.0173	B
2	0.10	100	0.1159	0.0392	B
3	0.05	260	0.1085	0.0425	B
4	0.10	260	0.1577	0.0523	B
5	0.05	347	0.1273	0.0422	B
6	0.10	347	0.1735	0.0612	B
7	0.05	520	0.1372	0.0553	B
8	0.10	520	0.1739	0.0770	B
9	0.05	1910	0.2001	0.1056	S
10	0.10	1910	0.2731	0.1349	S

where note π_4 as the term describing the target-to-impactor density dependency on crater scaling. At this stage, it is worth investigating this dependency first, as the highest δ is an order of magnitude higher than the lowest δ considered. Fig. 5 below shows normalised crater radius π_R as a function of π_4.

The π_R values at the impacts at 5 cm/s lie between 2 and 2.5, whereas for the 10 cm/s impact cases, they lie between 2.75 and 3.25. Qualitatively, there is not a discernible δ-dependency for the range of π_4 values between 1 and approximately 10. This could be confirmed by a fitting function as well. By assuming a constant K_{π_2} such that $K_{\pi_2} \approx K_R\pi_2^{-\alpha}$ (Housen and Holsapple, 2011), Eq. (14) can be rewritten as:

$$\pi_R = K_{\pi_2}\pi_4^{-\gamma} \tag{15}$$

Then, the curve-fitting results in a function in the following form:

$$\pi_R = 2.457\pi_4^{-0.052} \tag{16}$$

The γ exponent is found to be equal to 0.052, suggesting a weak dependency on the impactor density. In a recent study, the authors of this paper reported no discernible density dependency in impacts onto glass-beads-like material, with a γ = 0.07 (Çelik et al., 2022). Given the relatively limited set of simulations here, it cannot be conclusively stated that the density dependency is non-existent, but it may be less discernible in the impact regime considered here and warrants further studies on the subject. Nevertheless, given the results available here and the literature, hereafter it will be assumed that the impactor density

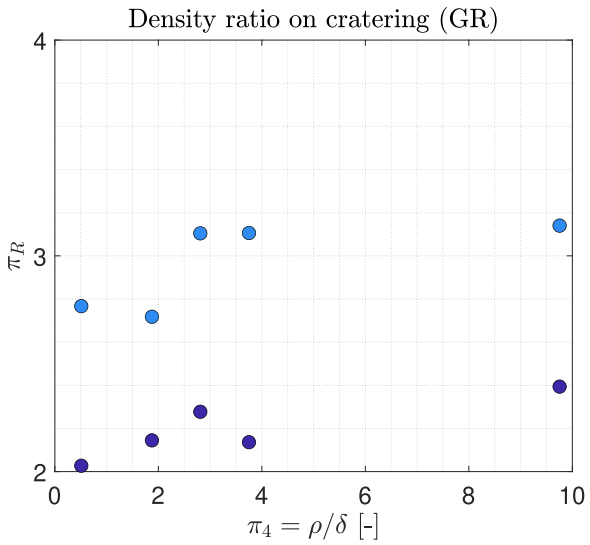

Fig. 5. Density dependency on crater scaling with gravel-like material. Darker and lighter blue data points are simulations with 5 and 10 cm/s impact speeds, respectively. (For interpretation of the references to colour in this figure legend, the reader is referred to the web version of this article.)

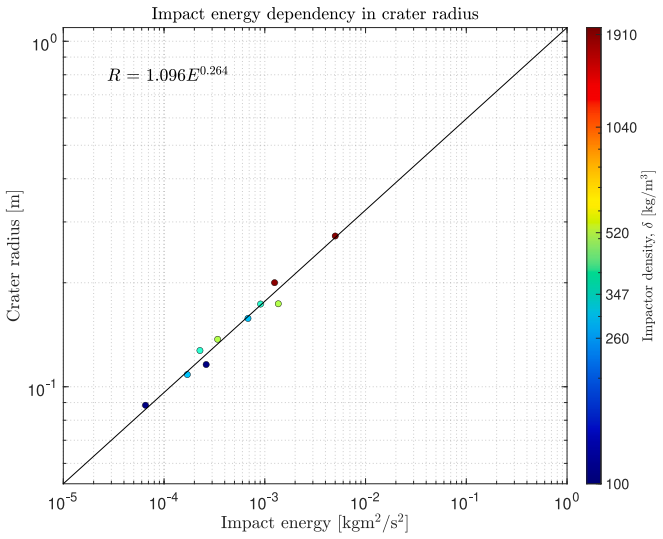

Fig. 6. Crater radius as a result of impact energy in GR type material. Colours denote individual impactor density values.

does not affect the cratering results and will be omitted from Eq. (14). The π_R relation will then take the following form:

$$\pi_R = K_R \pi_2^{-\alpha} \tag{17}$$

where $K_R \approx K_R \pi_4^{-\gamma}$, as per the earlier discussion. The curve fitting to the data would result in a relationship in the form as:

$$\pi_R = 0.567 \pi_2^{-0.217} \tag{18}$$

From Eq. (13), the following relationship can then be found:

$$\mu = \frac{-2\alpha}{1-\alpha} \tag{19}$$

Finally, μ is found after substituting α, such that:

$$\mu = 0.55 \tag{20}$$

Substituting μ in the exponent of π_4, i.e. $\frac{-6\nu+2+\mu}{3(2+\mu)}$ from Eq. (8) results in $\nu = 0.358$. This again suggests a weak impactor-density dependency, as per the discussion provided Housen and Holsapple (2011) where the empirically value $\nu = 0.4$ corresponds to no dependency of impactor density on cratering (Housen and Holsapple, 2011).

The μ value found (0.55) is at the higher end of the admissible values ($1/3 \leq \mu \leq 2/3$), which suggests an impact-energy dependency in cratering (Housen et al., 1983). Therefore the crater radii estimated in this paper are shown against the corresponding impact energies in Fig. 6.

The estimated crater radii are related to the dimensional function of energy, i.e. $R = 1.096E^{0.264}$, where the crater radius R is in the units of metre and the impact energy E is in the units of Joule. The goodness of fit value (conventionally defined as R^2, and not to be confused by the square of the crater radius), is equal to 0.974. This relationship is consistent with the existing literature.

Another aspect of low-speed cratering that may be of interest is crater depth through depth-to-diameter ratio, whose results are presented in Fig. 7.

The depth-to-diameter ratio is found ranging between 0.097 and 0.247 and a mean value of 0.19, with a fitted relationship $d = 0.21D$, where D denotes the crater diameter. The root mean square error (RMSE) and the goodness of the fit (R^2) values are calculated as 0.0143 and 0.83, respectively.

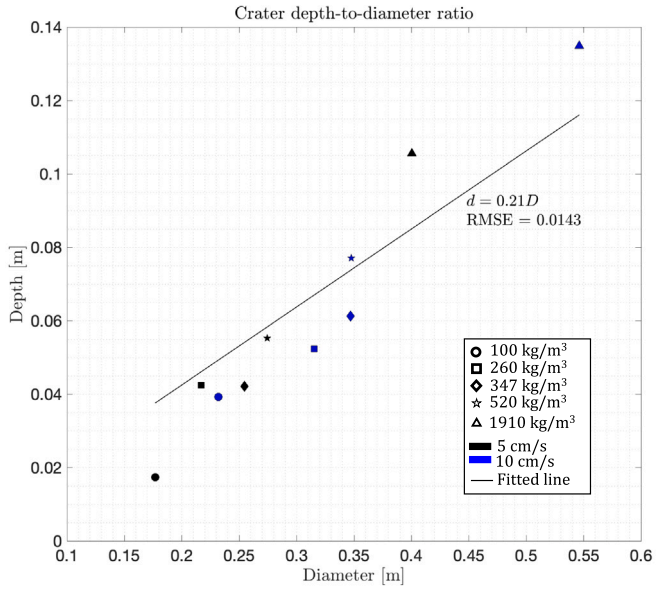

Fig. 7. Depth-to-diameter ratio in different simulations in GR type material.

Before discussing the wider implications of these cratering results, it is also worth investigating ejecta properties. Fig. 8 shows the scaled ejecta speed in the simulations with GR-like materials.

The expected ejecta speed scaling profile is obtained even at very small craters. The scaling is expected to fail near the impact point and towards the crater size and generally appears as the breaking of the power law region, shown in the inset in Fig. 8. It appears that the scaling continues beyond the crater radius, in fact almost up to the point twice the crater radius. Ejection beyond the crater radius was also observed in the same impacts in GB-like materials, but the power-law region appeared to break beyond the crater radius (Çelik et al., 2022). Ejection beyond the crater radius is observed in terrestrial low-speed impact experiments (Neiderbach et al., 2023), although the results here show that there may be cases where the scaling is still valid beyond the crater radius. This consideration may be important when interpreting ejecta from craters and at the impact locations of landed assets. As for ejection speeds, individual profiles will not be shown for conciseness, but the maximum particle-level ejection speed is found to

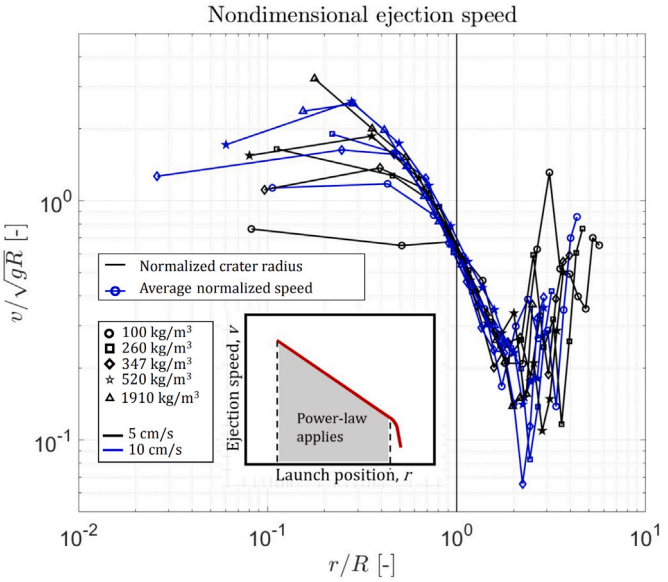

Fig. 8. Normalised ejection speed results of the impacts in GR type material. The black vertical line denotes the normalised crater radius. Insert figure shows expected qualitative appearance of the profile (Housen and Holsapple, 2011).

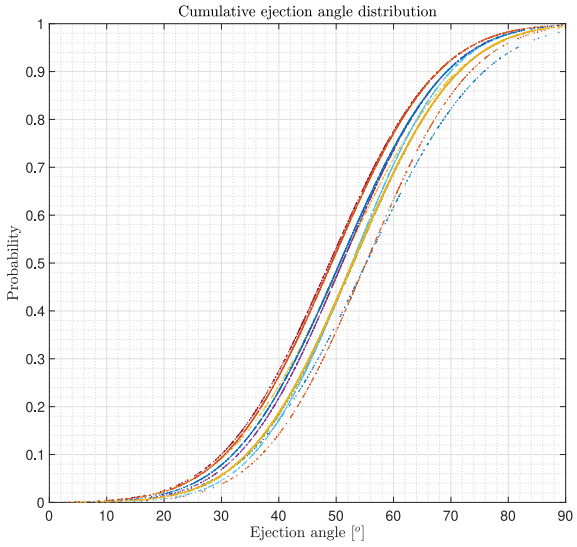

(a) Cumulative distribution of ejection angles

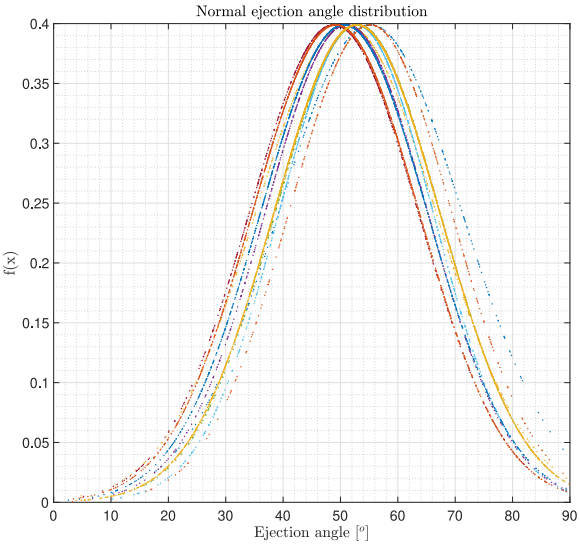

(b) Normal distribution of ejection angles

Fig. 9. Ejecta angle results. (a) Cumulative distribution of individual impact cases (b) Normal distribution of individual impact cases. f(x) denotes the probability density function for normal distribution. Each colour line represents a simulation in this work whose mean values are also presented in Fig. 10.

be approximately 4.5 cm/s at the impact case of $U = 10$ cm/s with an impactor density of $\rho = 1910$ kg/m^3, and a significant portion of the particles are ejected with speeds greater than 1 to 2 cm/s in all cases. Particles ejected at these speeds may be captured in asteroid systems.

In complex dynamical systems such as asteroids, the angle of ejection is an important property that governs the direction of particles that determines their escape or capture in the system. Fig. 9 below shows a normal distribution of the angle and the mean values of each simulation and the mean value for all simulations.

The mean ejection angle is found to be greater than typically assumed 45 deg and generally smaller for larger density impactors and vice versa. This may be related to smaller craters formed with lower density impactors although it is not entirely clear from Fig. 10 whether there is a clear correlation between the two.

Each ejected particle will finally contribute to the ejected mass from the impact process. This is considered from two different perspectives in this paper. The first is a more conventional crater-scaling perspective, in which, following the earlier discussion, the ejected mass faster than some ejecta speed v is investigated, both in normalised units, and shown in Fig. 11

The profile approximately follows the expected profile from crater-scaling relationships (Housen and Holsapple, 2011). Breaking of power-law scaling close to the impact point is represented well, even though the breaking towards the crater radius is less obvious. However, it should be noted that this representation of ejected mass could be misleading in some cases, as the ejection is shown to continue beyond the crater radius. Due to comparable effect of solar radiation pressure to gravity around asteroids, such material mobility can contribute to material loss and surface evolution in geological timescales, despite the low energy level. Therefore, this paper will also present the total mobilised material within and beyond the crater radius. This is an opportunity allowed by DEM simulations as the motion of each particle can be tracked. Particles moving in the positive z direction after the impact, with a speed greater than 0.1 mm/s are considered mobilised. The counting will then include many extremely low-energy particles but also a considerable number of particles that have speeds comparable to the impact speed. Table 6 then presents the total number of particles mobilised in each impact cases. As expected, the number of particles mobilised increases as the impactor density increases, as a result of increased impact energy and crater size. However, it may be rather unexpected that the number of particles mobilised beyond the crater size is always larger than that of within the crater bowl. Evidently, the mobilised particles in those regions have much lower energies than those close to the impact point due to lower ejection speeds, as shown in Fig. 8. However, the number found is as high as double the number of particles ejected within the crater. The number of particles ejected within the crater bowl can be as few as 43 to as high as 1905, depending on the impactor density and impact speed. Similarly, those mobilised beyond the final crater size vary between 268 and 2511. According to Table 6, as high as 30 kg of particles may be mobilised from the surface, approximately 13 kg from the final crater itself. At lower speeds and generally in the rebound cases, this value decreases, down to approximately 300 grams from the crater bowl and 2 kg in total.

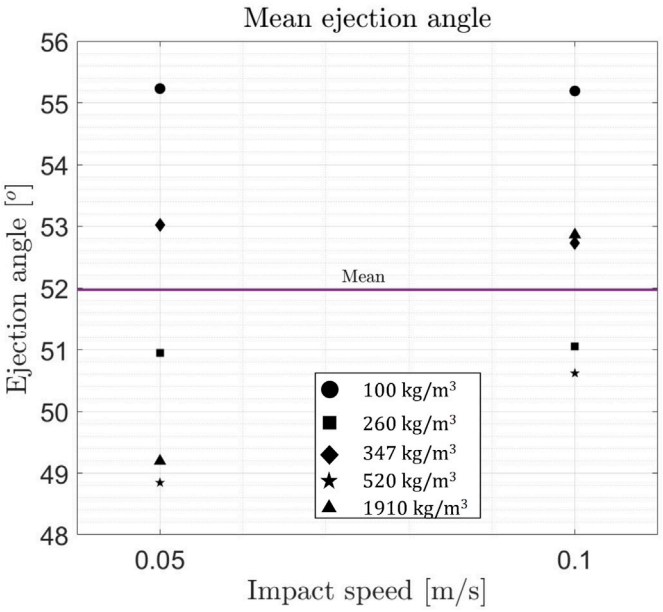

Fig. 10. Mean values in each impact case and the mean value in all impacts, denoted with a horizontal line.

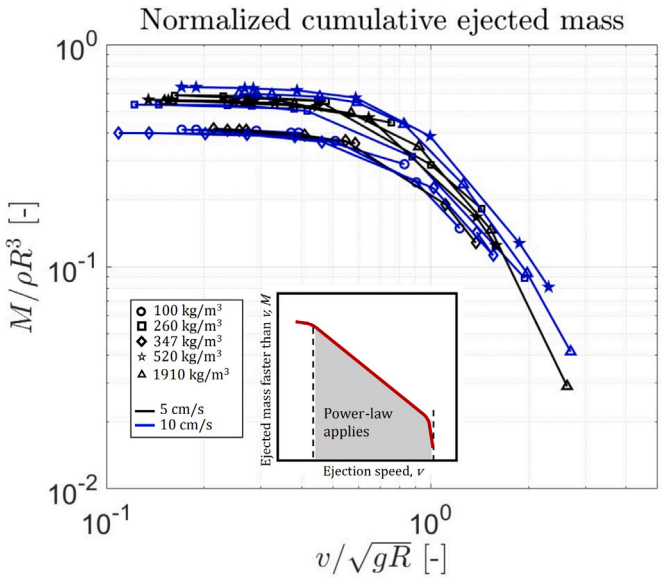

Fig. 11. Profile of normalised ejected mass. Inserted figure shows expected qualitative profile (Housen and Holsapple, 2011).

Now that the detailed results are presented for low-speed impact cratering with gravel type material, this may be compared against the cratering results with glass beads material simulations as presented in Çelik et al. (2022).

4.4. Comparisons with glass beads like material

Crater size scaling: In terms of crater scaling, GR-like materials are anticipated to behave similarly to more realistic materials as opposed to smooth GB-like materials. This was observed in general with smaller craters due to the increased strength mentioned earlier. However, the crater-scaling exponent, μ is found to be 0.55 which is similar to GB-like materials, $\mu = 0.56$ (Çelik et al., 2022). μ found here is higher than the typically considered value, ~0.4 for high-energy cratering in terrestrial experiments, but certainly not unobserved. The individually scaled crater radii π_R and π_2 parameters alongside the fitting function in both of these sets of simulations are presented in Fig. 12.

Table 6
Number of ejected particles. IN and OUT denote the number of particles ejected from inside and outside the region defined by the crater bowl, respectively. Similarly, M_{IN} denotes the mass of particles ejected from inside and M_{tot} denotes the total mass of the ejected particles, respectively.

δ [kg/m^3]	U [cm/s]	# (IN/OUT)	M_{IN} [kg]	M_{tot} [kg]
100	5	43/268	0.288	2.084
100	10	121/335	0.811	3.056
260	5	117/327	0.784	2.976
260	10	326/493	2.185	5.489
347	5	160/424	1.072	3.914
347	10	402/633	2.694	6.937
520	5	228/433	1.528	4.430
520	10	526/975	3.525	10.060
1910	5	696/1123	4.664	12.191
1910	10	1905/2511	12.767	29.596

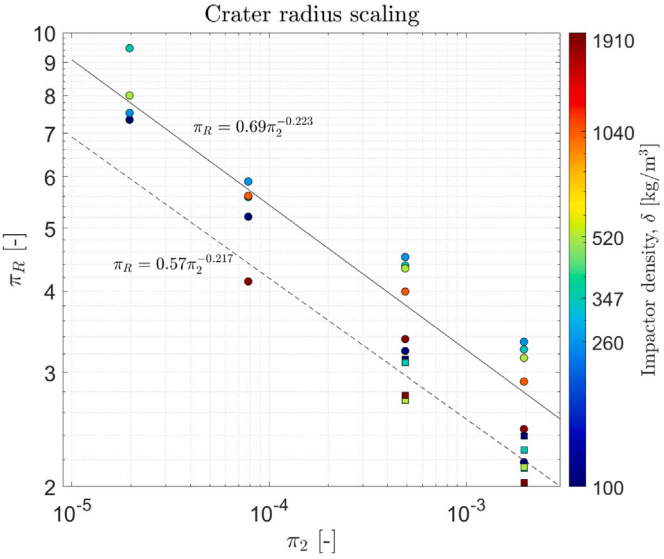

Fig. 12. Crater radius scaling results. Circle and square data points represent GB and GR materials, respectively. Black and dashed black lines are fitted relationships to the data for GB and GR type materials, respectively. Colours denote individual impactor density values for a given impact case. (For interpretation of the references to colour in this figure legend, the reader is referred to the web version of this article.)

Similarity in fitting functions is apparent. In gravel-like materials, the craters are smaller at the same impact, impactor, and target properties than those of glass-beads-like materials. But in this paper, it was found that higher dissipation in material properties only changes the linear multiplier, but does not change the exponent significantly. The variation in impactor density does not seem to affect the crater size scaling in GR-like materials, which was shown through $\nu = 0.358$ value. This was also the case observed with GB-like materials (Çelik et al., 2022). The lack of impactor density dependency in crater size scaling in both GR- and GB-like materials, especially considering the order of magnitude difference (19.1 times) between the lowest and highest impactor density, is noteworthy, but the set of simulations is still relatively small (a total of 31) and warrants further studies on the impactor density dependency. In terms of impact energy dependency of crater sizes, $R = 1.096E^{0.264}$ is found in GR-like material. A similar function is previously found as $R = 1.014E^{0.217}$ in GB-like material (Çelik et al., 2022). The energy dependency found here is consistent with the majority of low-speed cratering studies, as it will be discussed later.

In the simulations with GB-like material, the mean depth-to-diameter ratio of craters is found to be approximately 0.13 with values between 0.09 and 0.22. The mean value was 0.145 (Çelik et al., 2022). While the range of values is similar in both GB- and GR-like material simulations, the ratio is approximately 1.6 times higher for GR-like materials. This is mostly due to smaller crater diameters in GR-like materials, rather than deeper craters.

Ejecta properties: The maximum ejection speed is found to be below 5 cm/s with GR-like materials and at the greatest impactor density and speed (i.e., δ = 1910 kg/m^3 and U = 10 cm/s). In comparison, for the same case the maximum found in GB-like materials is approximately 10 cm/s (Çelik et al., 2022). The difference may be explained by the exaggerated cratering behaviour due to smoother materials (Housen and Holsapple, 2011). It may be expected that at higher speeds and denser object result in higher speed ejecta.

In GB-like materials, the mean ejection angle is also found greater than 45 deg in all cases, with the overall mean slightly higher than that of here with 53 deg (Çelik et al., 2022). Note, however, that study had two other simulation cases at 25 cm/s and 50 cm/s, where the mean value is higher (Çelik et al., 2022). Neither in GB-like materials nor in GR-like materials here, there is an obvious trend of the mean ejection values with impact cases. Nevertheless, it can be argued that, relatively higher values of ejection angles at lower-density impactors are a result of small craters where the ejection does not extend well beyond the impact craters in GR-like material. The similarity of mean values at δ = 100, 260 and 347 kg/m^3 impactors at both impact speeds (~56, ~51 and ~53 deg, respectively) are also noteworthy, even though their probability distribution appears to be separated in the left figure of Fig. 9. These are all rebound cases, with relatively small craters and small numbers of mobilised particles, which may explain the higher ejection angles. In the remaining two impact speeds, where one is a rebound case and the other is a submerge case, the mean angle appears to increase with the impact speed, which may be explained by increasing crater size as a result of increasing impact energy, leading to higher ejection angles for particles.

As for ejected quantity of material the number of particles ejected is higher in both from inside and outside of the final crater radius in GB-like material. This can be explained with the exaggerated impact behaviour, both in crater size and ejection properties in smoother materials (Housen and Holsapple, 2011). For comparison, in U=10 cm/s - δ=1910 kg/m^3 case, the ejected mass from crater bowl is approximately 15 kg in GB-like material, whereas it is 13 kg in GR-like material. It is worth reiterating that only a fraction of the number of particles in Table 6 would potentially orbit around or escape from a small asteroid, but even then a considerable mass may be launched. These results will have implications for both understanding small-body environments and designing space missions that explore them.

5. Comparisons with other studies

The coefficient of restitution: The ϵ values calculated here are lower than that of an observed ricochet event in Bennu, where a value of 0.57 is estimated (Chesley et al., 2020). While the impact and impactor properties may not necessarily be comparable, the particle on Bennu impacted with a tangential velocity component, at a 67 deg angle from the local horizontal plane (Chesley et al., 2020). It is shown previously that oblique impacts have a higher coefficient of restitution values than those purely at local vertical (Çelik et al., 2019a), therefore lower values may be expected without accounting for any other effect at the impact. In the literature, the coefficient of restitution values in small body surfaces vary in a large range. In the Hayabusa mission's touchdown at 6.9 cm/s, a coefficient of restitution value of 0.85 is estimated (Yano et al., 2005). However, the reported value may be strongly affected by the sampling horn and its springs and may not be representative of actual asteroid surface. In the similar range of impact speeds, Brisset et al. (2018) reported ϵ values of 0.01 to 0.28 from different low-speed impact experiments (10–110 cm/s) onto cohesive sand under 10^{-2}-$10^{-4}g$ (Brisset et al., 2018; Colwell, 2003; Colwell et al., 2017). In ballistic landings, the ϵ value was estimated between 0.6 and 0.8 from the Hayabusa2 images in MINERVA-II landing at approximately 30 cm/s (Van wal et al., 2019). Again in the Hayabusa2 mission, the authors of this paper used the three-dimensional velocity magnitudes (highest impact at ~17 cm/s) and impact events reported for the MASCOT lander (Scholten et al., 2019) in Eq. (12) to estimate the coefficient of restitution values between 0.3 and 0.98 and in an increasing trend with decreasing impact speed similar to those found here. However, it is important to note that the coefficient of restitution is also highly dependent on impact angle, attitude and rotation for MASCOT's cuboid shape, and non-spherical shapes in general (Van wal et al., 2021). Both in Maurel et al. (2018) in the impact simulations of MASCOT and Çelik et al. (2019a) for non-spherical landers that vertical impacts mostly resulted in submerging in the absence of attitude rotation under microgravity. Reporting on no-initial-spin cases, Maurel et al. (2018) found some cases of rebound with ϵ of approximately 0.1 and up to 0.35 with spin. ϵ is also reported between 0.0–0.25 in no-boulder granular beds, with an initial spin at the impacts (Thuillet et al., 2018). For higher impact speeds on the order of m/s in small-body environments, Durda et al. (2012) estimated the coefficient of restitution of Eros' surface in between 0.09–0.18 on average in different craters, with individual cases as high as 0.29. The variability in the coefficient of restitution values is therefore very large, and covers almost the full range of possible values between 0 and 1. Nevertheless, the values calculated here are closer to those reported by Brisset et al. (2018, 2020) and Durda et al. (2012). Brisset et al. (2018, 2020) studies consider only vertical impacts and in fact, gravity levels as low as that of Eros (i.e., ~$10^{-4}g$), even though with a cohesive granular material. However, it may still be more representative of the results presented in this paper.

Crater scaling: Some of the experimental studies under reduced gravity and lower speed impacts, as well as reduced atmospheric pressure, seem to exhibit higher μ values than typically assumed 0.4 for dry granular materials, some as high as the values found here (Cintala et al., 1989; Kiuchi et al., 2019). While there need to be further studies performed to constrain the values, higher μ values may be a property of the impact regime itself.

It is discussed in Çelik et al. (2022) that more dissipative particles would likely result in μ values closer to the values expected from higher energy cratering, $\mu \sim 0.4$. This was also stated in a DEM-based impact cratering study by Wada et al. (2006) and implied in Housen and Holsapple (2011) that impact craters in GB-like materials have more exaggerated properties, both in size and ejecta speed. Wada et al. (2006) considered impact studies greater than 100 m/s and found μ closer to 0.4. However, at similar impact speeds, Tsujido et al. (2015) found μ = 0.56, closer to the one found here. Tsujido et al. (2015) also considered a large variation in impactor density and found a little dependency. Under low gravity and low atmospheric pressure (0.83 atm), Cintala et al. (1989) found μ = 0.444 at 65 to 130 m/s impacts. Kiuchi et al. (2019) considered much lower impact speeds and found μ value between 0.44 and 0.56. Kiuchi et al. (2019) is potentially the most relevant study to this paper, as the authors both considered a lower gravity and lower impact speed, as well as lowered atmospheric pressure, and found no impactor density dependency and μ similar to that of found here.

It is worth considering these results in the context of some of the existing crater size scaling results in both high- and low-speed impacts under terrestrial or low gravity, as shown in Fig. 13.

The figure shows crater size scaling results of several experimental studies, initially discussed in Çelik et al. (2022). The blue reference line is by using impact and target properties from Takizawa and Katsuragi (2020), by using generic parameters K_1 = 1.03, μ = 0.41 and ν = 0.4 from Holsapple and Housen (2007). The black dotted reference line

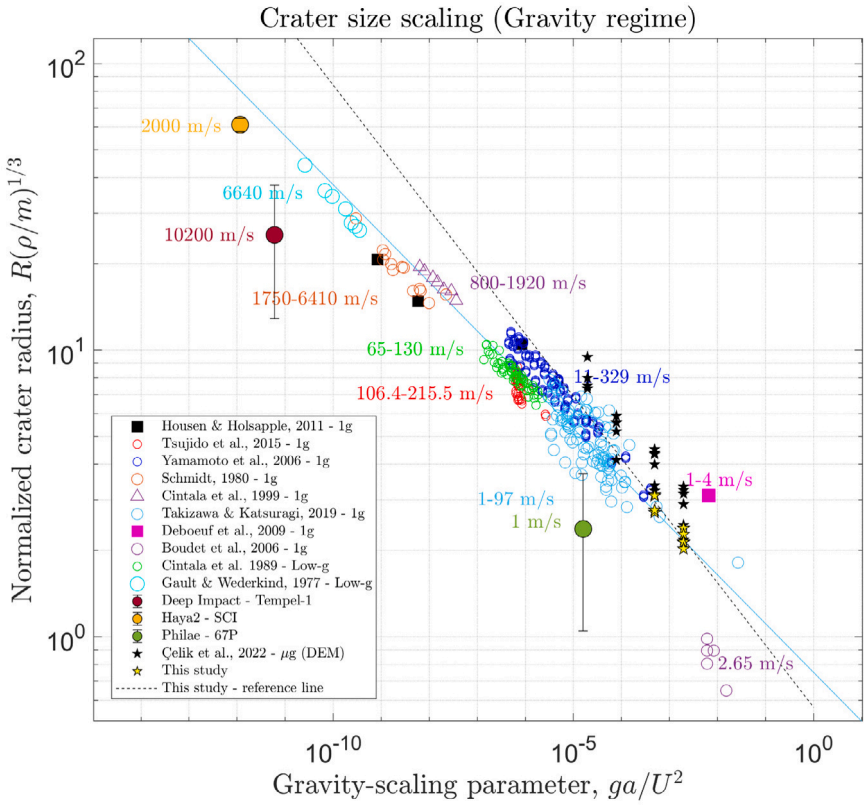

Fig. 13. Crater size scaling results from previous experimental studies, together with the DEM simulations with gravel-like material in this study and glass beads-like material from Çelik et al. (2022). Light blue solid line is drawn as a reference with target properties from Takizawa and Katsuragi (2020) and generic cratering parameters $K_1 = 1.03$, $\mu = 0.41$ and $\nu = 0.4$ from Holsapple and Housen (2007). (For interpretation of the references to colour in this figure legend, the reader is referred to the web version of this article.)

is drawn with the results here. The figure also includes crater size scaling results with GB-like from Çelik et al. (2022). The scaled craters in this study fit within the region bounded by previous experimental studies despite the greater μ value found. This is further evidence of the applicability of crater scaling in this regime and the validity of the results presented in this paper.

Housen and Holsapple (2011) have previously shown a δ-dependency in three different high-speed impact experiments where the impact speed is higher than 1 km/s. However, likely in a more relevant impact regime, Tsujido et al. (2015) considered a set of impactors whose densities vary by an order of magnitude and impact speeds a few hundreds of m/s. Tsujido et al. (2015) also identified a weak impactor-density dependency, albeit they obtain a higher γ value (~0.11), and concluded that it may be due to relatively low speed impacts. Tsujido et al. (2015) considered much lower impact speeds (1 to 4.6 m/s) under $0.2g$ to $1g$ and found almost no dependency to impactor density.

As for impact energy dependency, De Vet and De Bruyn (2007) found the exponent of energy as 0.226 when scaled with crater volume for impact experiments in dry granular material at 0.6–4.4 m/s at $1g$, although the authors also included a term representing particle size in the functional relationship. In a different set of low-speed (~5 m/s) experiments with different dry granular materials, Dowling and Dowling (2013) also found a similar exponent here, but the crater size is measured from rim to rim. Takizawa and Katsuragi (2020) reported the exponent as approximately 0.19. The results obtained here are higher than Takizawa and Katsuragi (2020) but it is consistent with impact-energy scaling as a result of the μ value Holsapple and Schmidt (1982), which is confirmed by a quarter-root energy scaling, expressed as $R = 1.097E^{-0.264}$.

In the cratering literature, the depth-to-diameter ratio is also varied in a large range depending on the impact, impactor, and target conditions. For very large-scale cratering events, Melosh (1989) states that the ratio would be approximately 0.25–0.35. For lower energy events, Tsujido et al. (2015) reported higher values, 0.35–0.4 at approximately 200 m/s impacts for very small craters generated by mm-sized projectiles. The values closer to the one found here are reported in Yamamoto et al. (2006) at 0.11–0.14 for 11–329 m/s impacts. Thuillet et al. (2020)'s reported range of 0.3–0.35 is found under low-gravity conditions but attributed the results to incomplete cratering.

In small asteroids, the ratio is reported as 0.08 ± 0.03 (range 0.01–0.15) for Itokawa (Hirata et al., 2009) and 0.09 ± 0.02 (range 0.03 to 0.15) for Ryugu (Noguchi et al., 2021). Neither dataset has craters as small as those investigated here, but the mean ratio reported for smaller craters of Ryugu (diameter<25 m) 0.06 ± 0.02 (range 0.03–0.09) (Noguchi et al., 2021). Noguchi et al. (2021) also note that in smaller craters (diameter<50 m), the ratio tends to increase as the crater diameter increases, which is also the observation in Fig. 7.

At OSIRIS-REx target Bennu, the ratio is calculated to be 0.10 ± 0.03 with a range between 0.02 to 0.19 for craters larger than 10 m in diameter (Daly et al., 2020). Daly et al. (2020) also investigated small craters of Bennu (<10 m and as small as ~1 m) which are potentially more relevant to this study. They found the mean ratio 0.13 ± 0.04 in a range 0.04–0.27 (Daly et al., 2022). The mean ratio reported by Daly et al. (2022) is almost exactly the value (including the range) that was found in Çelik et al. (2022) with simulations in GB-like material. Similarly the estimated range with the impacts in GR-like material also matches with the results of Daly et al. (2022), albeit with a higher mean ratio in this paper. Moreover, the same study also noted the presence of boulders near Bennu's small craters with sizes more than half of the crater diameters (Daly et al., 2022). Similar impact outcomes are also displayed in this paper in Fig. 3. The apparent similarity between

the observational results on Bennu and this paper is encouraging for observable low-speed impact activity in small solar system bodies.

Ejecta properties: For a relevant comparison with ejection speeds in low-speed impact cratering, Chesley et al. investigated the trajectories of some 313 particles around Bennu with speeds varying between 0.07 m/s and 3 m/s (Chesley et al., 2020). Such number of particles is approximately counted in a single impact case in this paper, in which the highest ejection speed found is approximately 0.045 m/s. This is lower than Chesley et al. (2020) but similar to those reported in Lauretta et al. (2019) for Bennu.

It is typically assumed in the literature that the mean ejecta angle is 45 deg (Richardson et al., 2007). It is also argued in Cintala et al. (1999)'s impact experiments, in which the ejecta was recorded in high-speed cameras, that ejecta angle varies approximately around 45 deg. It has been observed previously that ejecta angle is higher (measured from local horizontal) close to the impact point, almost jetting like with near 90 deg ejections and roughly decreases towards the crater radius (Housen and Holsapple, 2011). Here, it is observed that the mean ejection angle is always greater than 45 deg, and higher than 55 deg for the lowest δ cases. The overall mean ejection angle is 52 deg. The ejection profiles can be described as normal distributions where standard deviations vary between 11 deg–15 deg in different cases.

6. Discussion

Of the 10 simulations in gravel-like material, 8 simulations resulted in a rebound. The rebound behaviour is previously observed in local vertical impacts (Brisset et al., 2020; Katsuragi and Blum, 2017), but those reports have all been with materials that possess some cohesive strength, here it was shown that it may also occur in dry granular materials. The rebound behaviour can be explained by the frictional strength in gravel-like materials.

As for the craters sizes ejecta from the impact craters, it was shown that it follows the scaling relationship as previously demonstrated (Çelik et al., 2022). The ejected particles have speeds at the lower end of ejected (and tracked) particles of Bennu (Lauretta et al., 2019; Chesley et al., 2020) in both gravel and glass beads like materials, hence may be of interest in interpreting these events. Related to this point, the number of particles mobilised beyond the final crater volume is higher than that of within. Therefore, a considerable quantity of mass may be mobilised by a low-speed impactor within and beyond the final crater bowl, ranging from a few hundred grams to a few tens of kilogrammes depending on the impact case. Combined with the ejection speed results, some materials may be ejected while others orbiting and eventually re-impacting. These possible events may lead to a variety of changes in a small body in geological timescales (Scheeres et al., 2019, 2020b). Material loss through the escape of particles may change the orbit of the body, whereas a preferential direction in ejection may lead to a change in rotation period, though more likely in oblique impacts (Scheeres et al., 2020b). Ejection may therefore be an additional contributing process (Scheeres et al., 2020b; Vance et al., 2022). Of the particles that have enough energy to have a trackable (sub-)orbital motion, higher resolution gravity may be extracted by tracking their motion (Chesley et al., 2020), which may give an indication on the internal structure of the body (Scheeres et al., 2020a).

Further to crater sizes, the crater depth-to-diameter (d/D) ratio also has similarities with observational findings. In simulations with GR-like material, the crater d/D ratio is found to be 0.21. It is higher than that of small craters (as small as ~1 m) of Bennu (d/D =0.13 ± 0.04), but the range of values (0.097–0.24) found here is within that of Bennu (0.04–0.27) (Daly et al., 2022). Crater degradation over time generally reduces the d/D ratio, and the craters here can only be representative of fresh craters. The craters in this study are still at least an order of magnitude smaller than those of Daly et al. (2022). Nevertheless, small craters could be generated by either small but very high-energy impactors, such as meteoroids, or larger but low-energy impactors as per the crater scaling, such as those in this paper. Indeed, there may be signs of the latter within or near the small craters of Bennu. Daly et al. discuss that there are small boulders near the small craters whose size ratio with respect to crater size is greater than 0.5, i.e. the impactors have more than half the size of the craters (Daly et al., 2022). Two such examples are shown in two of Bennu's small craters in Fig. 14. Similarly, dimple-like structures in Itokawa's Sagamihara and Muses Sea regions also have boulders at the bottom of craters, whose sizes are 0.25–0.5 times the size of crater diameters, which may be created by the impacts of those boulders at speeds below the escape speed of Itokawa (~0.17 m/s) (Kiuchi et al., 2019).

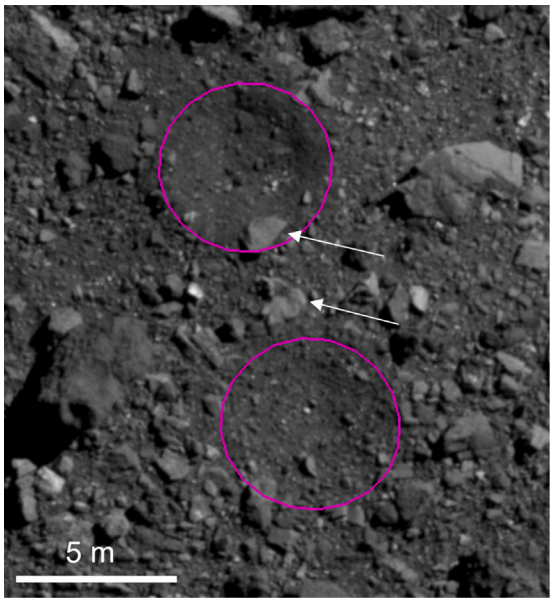

Fig. 14. Two example small craters on Bennu (Image credit: NASA/OSIRIS-REx/UA/OCAMS). Arrows point to possible impactors close to small craters.

The qualitative impact outcomes presented in Fig. 3 have displayed similarities with Bennu's small craters seen in 14, where the impactors either submerged but stayed in the final crater wall, or rebounded but landed nearby. Some of those outcomes in Fig. 3 are a result of low-mass impactors, which would require high porosity boulders, assuming that their density is similar to that of target density. Sakatani et al. (2021) discuss that boulders of as high as 70% porosity are present in the floors of fresh small craters (<20 m-diam) of Ryugu, even though this may be intrinsic to the surface, rather than created by some impact process (Sakatani et al., 2021). It is also possible that boulders may be launched as a result of a larger impact (Nakamura et al., 2008) or some other process, such as seismic shaking, which may strand large boulders on the surface but may allow smaller ones to launch (Wright et al., 2020a; Tancredi et al., 2012, 2022).

The pre- and post-impact predictions of the outcomes of DART impact on Didymos have shown that some of the launched boulder may have impacted on Didymos or its companion Dimorphos (Rossi et al., 2022; Kareta et al., 2023; Moreno et al., 2024; Langner et al., 2024). While the studies rely on various assumptions in dynamical model, boulder sizes and its properties, all predictions suggest the outcome of re-impact of one of the two bodies. The numbers vary between a few tens of boulders up to ten thousand and impact speeds from a few cm/s to up to a m/s, which are dependent on the model and the simulation setup (Rossi et al., 2022; Moreno et al., 2024; Langner et al., 2024). A potential evidence of a re-impact activity was in fact shown through telescopic observation of the dust tail following the DART impact (Kareta et al., 2023). The dimming in the dust tail brightness

paused after the first eight days, the brightness increased again before dimming. The most plausible explanation is found to be a re-impact of a boulder and release of material afterwards (Kareta et al., 2023). Combined with the simulations and considering low escape speed (a few cm/s) of Didymos-like object, such impacts can only happen at speed ranges similar those in this paper. It may therefore be possible to observe the traces of these impacts, especially in smoother regolith covered regions, upon the arrival of Hera mission (Michel et al., 2025). The images from DART mission suggest that equatorial regions of Didymos may harbour such regolith covered region similar to asteroids Ryugu and Bennu (Chabot et al., 2024). Crater size-frequency distributions may need to account for these secondary cratering activities. The secondary craters will also likely expose fresh materials on the surface, which may present an opportunity to compare against space weathered surface.

The results presented in this paper have implications for missions that interact with the surfaces of their targets, as well. Indeed, every low-energy ballistic landing and touchdown on a small body is are examples of low-speed impact (Ballouz et al., 2021). Hence, the conditions leading to rebound behaviour may be used to constrain bouncing motion of small ballistic landers and to characterise small-body surfaces (Murdoch et al., 2021). Moreover, ejected material during landing, sampling and hovering operations may damage the spacecraft or its instruments, as reported for one of the cameras during Hayabusa2 touchdown on Ryugu (Kouyama et al., 2021). Craters and their ejecta properties (speed, angle and mass) as found here can be used for safeguarding strategies to protect spacecraft (and its equipment) during those operations. Alternatively, the same knowledge can be used to devise novel sampling strategies from orbit or without touchdown by mobilising surface material via small low-speed impactors. Such missions may be of lower cost and of interest for asteroid prospecting missions and planetary science missions in general.

7. Conclusion

Recent small-body exploration missions have demonstrated existence of potential low-speed impact activity on regolith covered surface of asteroids. Such low-speed impacts are similarly of interest from space engineering perspective, as the bouncing motion of small landers, landing and sampling operations on larger spacecraft on small bodies can also be characterised in a similar way. In this work, discrete element method simulations are used with gravel-like realistic material to simulate the cratering process in ~cm/s low-speed regime under microgravity found at small asteroids. The simulation results are discussed in comparison with the results of simulations with smoother glass beads-like material, broader experimental literature and observational findings from small-body exploration missions

The results show that most impacts in gravel-type material rebound off the surface. While rebounds have been observed in this regime previously, it is confirmed further that it can also be observed in non-cohesive material and impacts to local vertical as well. The increased strength due to more frictional gravel-like material results in higher density objects to be rebound, as opposed to glass-beads-like material. The resulting craters are smaller in gravel-like materials than in glass-beads-like materials, which may be expected due to the increased frictional strength, but the resulting crater size scaling exponent is similar in both materials ($\mu \approx 0.55$) and does not seem to be affected by impactor's density. Nevertheless, the craters in gravel-like materials in this regime appear to align much better with the experimental studies in the literature which confirms the applicability of crater scaling relationships in the considered regime. Ejecta properties similarly follow the scaling relationships. However, material mobility after an impact extends beyond crater dimensions. More particles are mobilised beyond the crater boundaries compared to within. The impact outcomes demonstrate similarities with OSIRIS-REx target asteroid Bennu's small craters. The depth-to-diameter ratios of the craters in both gravel and glass-beads-like materials are found within the range of small craters of Bennu. The similarities between final impactor positions within and in the vicinity of the simulated impact craters and the images of boulders near small craters of Bennu may indicate a low-speed impact activity and craters formed as a result.

The simulations performed with more realistic material properties help build confidence in applying crater scaling relationships in low-speed impacts under microgravity. It is evident that further studies will be necessary to constrain scaling coefficients and understand various dependencies of cratering in this regime. Nevertheless, the results presented shed light on the potential low-speed impact on small bodies and may aid in the design of surface operations of space missions.

CRediT authorship contribution statement

Onur Çelik: Writing – review & editing, Writing – original draft, Visualization, Validation, Software, Methodology, Investigation, Funding acquisition, Formal analysis, Data curation, Conceptualization. **Ronald-Louis Ballouz:** Writing – review & editing, Validation, Supervision, Software, Methodology, Investigation, Formal analysis. **Daniel J. Scheeres:** Writing – review & editing, Validation, Supervision, Resources, Investigation, Conceptualization. **Yasuhiro Kawakatsu:** Writing – review & editing, Supervision, Resources, Methodology, Funding acquisition.

Declaration of competing interest

The authors declare that they have no known competing financial interests or personal relationships that could have appeared to influence the work reported in this paper.

Acknowledgements

Onur Çelik is partially supported by the Japanese Government Research Scholarship and SOKENDAI Student Dispatch Programme for his visit to CU Boulder during this study.

Data availability

Data will be made available on request.

References

Arakawa, M., Saiki, T., Wada, K., Ogawa, K., Kadono, T., Shirai, K., Sawada, H., Ishibashi, K., Honda, R., Sakatani, N., Iijima, Y., Okamoto, C., Yano, H., Takagi, Y., Hayakawa, M., Michel, P., Jutzi, M., Shimaki, Y., Kimura, S., Mimasu, Y., Toda, T., Imamura, H., Nakazawa, S., Hayakawa, H., Sugita, S., Morota, T., Kameda, S., Tatsumi, E., Cho, Y., Yoshioka, K., Yokota, Y., Matsuoka, M., Yamada, M., Kouyama, T., Honda, C., Tsuda, Y., Watanabe, S., Yoshikawa, M., Tanaka, S., Terui, F., Kikuchi, S., Yamaguchi, T., Ogawa, N., Ono, G., Yoshikawa, K., Takahashi, T., Takei, Y., Fujii, A., Takeuchi, H., Yamamoto, Y., Okada, T., Hirose, C., Hosoda, S., Mori, O., Shimada, T., Soldini, S., Tsukizaki, R., Iwata, T., Ozaki, M., Abe, M., Namiki, N., Kitazato, K., Tachibana, S., Ikeda, H., Hirata, N., Hirata, N., Noguchi, R., Miura, A., 2020. An artificial impact on the asteroid 162173 Ryugu formed a crater in the gravity-dominated regime. Science 1701 (March), http://dx.doi.org/10.1126/science.aaz1701.

Ballouz, R., 2017. Numerical Simulations of Granular Physics in the Solar System (Ph.D. thesis). University of Maryland, College Park.

Ballouz, R.L., Richardson, D.C., Michel, P., Schwartz, S.R., Yu, Y., 2015. Numerical simulations of collisional disruption of rotating gravitational aggregates: Dependence on material properties. Planet. Space Sci. 107 (1), 29–35. http://dx.doi.org/10.1016/j.pss.2014.06.003.

Ballouz, R.-L., Walsh, K.J., Sánchez, P., Holsapple, K.A., Michel, P., Scheeres, D.J., Zhang, Y., Richardson, D.C., Barnouin, O.S., Nolan, M.C., Bierhaus, E.B., Connolly, Jr., H.C., Schwartz, S.R., Çelik, O., Baba, M., Lauretta, D.S., 2021. Modified granular impact force laws for the OSIRIS-REx touchdown on the surface of asteroid (101955) Bennu. Mon. Not. R. Astron. Soc. 507 (4), 5087–5105. http://dx.doi.org/10.1093/mnras/stab2365.

Biele, J., Ulamec, S., Maibaum, M., Roll, R., Witte, L., Jurado, E., Munoz, P., Arnold, W., Auster, H.-U., Casas, C., Faber, C., Fantinati, C., Finke, F., Fischer, H.-H., Geurts, K., Guttler, C., Heinisch, P., Herique, A., Hviid, S., Kargl, G., Knapmeyer, M., Knollenberg, J., Kofman, W., Komle, N., Kuhrt, E., Lommatsch, V., Mottola, S., Pardo de Santayana, R., Remetean, E., Scholten, F., Seidensticker, K.J., Sierks, H., Spohn, T., 2015. The landing(s) of Philae and inferences about comet surface mechanical properties. Science 349 (6247), 1–6. http://dx.doi.org/10.1126/science.aaa9816.

Bottke, W.F., Moorhead, A.V., Connolly, H.C., Hergenrother, C.W., Molaro, J.L., Michel, P., Nolan, M.C., Schwartz, S.R., Vokrouhlický, D., Walsh, K.J., Lauretta, D.S., 2020. Meteoroid impacts as a source of Bennu's particle ejection events. J. Geophys. Res.: Planets 125 (8), http://dx.doi.org/10.1029/2019JE006282.

Boudet, J.F., Amarouchene, Y., Kellay, H., 2006. Dynamics of impact cratering in shallow sand layers. Phys. Rev. Lett. 96 (15), 1–4. http://dx.doi.org/10.1103/PhysRevLett.96.158001.

Brisset, J., Colwell, J., Dove, A., Abukhalil, S., Cox, C., Mohammed, N., 2018. Regolith behavior under asteroid-level gravity conditions: low-velocity impact experiments. Prog. Earth Planet. Sci. 5 (1), 73. http://dx.doi.org/10.1186/s40645-018-0222-5.

Brisset, J., Cox, C., Anderson, S., Hatchitt, J., Madison, A., Mendonca, M., Partida, A., Remie, D., 2020. Regolith behavior under asteroid-level gravity conditions: low-velocity impacts into mm-and cm-sized grain targets. Astron. Astrophys. 642, A198. http://dx.doi.org/10.1051/0004-6361/202038665.

Buckingham, E., 1914. On physically similar systems; illustrations of the use of dimensional equations. Phys. Rev. 4 (4), 345. http://dx.doi.org/10.1103/PhysRev.4.345.

Çelik, O., Ballouz, R.-L., Scheeres, D.J., Kawakatsu, Y., 2022. Material dependency of crater scaling in low-speed impacts under microgravity. LPI Contrib. 2681, 2006.

Çelik, O., Ballouz, R.-L., Scheeres, D.J., Kawakatsu, Y., 2022. A numerical simulation approach to the crater-scaling relationships in low-speed impacts under microgravity. Icarus 377, 114882. http://dx.doi.org/10.1016/j.icarus.2022.114882.

Çelik, O., Baresi, N., Ballouz, R.-L., Ogawa, K., Wada, K., Kawakatsu, Y., 2019a. Ballistic deployment from quasi-satellite orbits around phobos under realistic dynamical and surface environment constraints. Planet. Space Sci. 178 (104693), http://dx.doi.org/10.1016/j.pss.2019.06.010.

Çelik, O., Karatekin, O., Ritter, B., Sánchez, J.P., 2017. Reliability analysis of ballistic landing in binary asteroid 65803 (1996 GT) didymos under uncertainty and GNC error considerations. In: 26th International Symposium on Spaceflight Dynamics. Matsuyama, Japan, June 3–9, Paper no. ISSFD-2017-031.

Çelik, O., Sanchez, J.P., 2017. Opportunities for ballistic soft landing in binary asteroids. J. Guid. Control Dyn. 40 (6), http://dx.doi.org/10.2514/1.G002181.

Çelik, O., Sánchez, J.P., Karatekin, Ö., Ritter, B., 2019b. A comparative reliability analysis of ballistic deployments on binary asteroids. Acta Astronaut. 156, 308–316. http://dx.doi.org/10.1016/j.actaastro.2018.03.020.

Chabot, N.L., Rivkin, A.S., Cheng, A.F., Barnouin, O.S., Fahnestock, E.G., Richardson, D.C., Stickle, A.M., Thomas, C.A., Ernst, C.M., Daly, R.T., Dotto, E., Zinzi, A., Chesley, S.R., Moskovitz, N.A., Barbee, B.W., Abell, P., Agrusa, H.F., Bannister, M.T., Beccarelli, J., Bekker, D.L., Syal, M.B., Buratti, B.J., Busch, M.W., Bagatin, A.C., Chatelain, J.P., Chocron, S., Collins, G.S., Conversi, L., Davison, T.M., DeCoster, M.E., Deshapriya, J.D.P., Eggl, S., Espiritu, R.C., Farnham, T.L., Ferrais, M., Ferrari, F., Föhring, D., Fuentes-Muñoz, O., Gai, I., Giordano, C., Glenar, D.A., Gomez, E., Graninger, D.M., Green, S.F., Greenstreet, S., Hasselmann, P.H., Herreros, I., Hirabayashi, M., Husárik, M., Ieva, S., Ivanovski, S.L., Jackson, S.L., Jehin, E., Jutzi, M., Karatekin, O., Knight, M.M., Kolokolova, L., Kumamoto, K.M., Küppers, M., Forgia, F.L., Lazzarin, M., Li, J.-Y., Lister, T.A., Lolachi, R., Lucas, M.P., Lucchetti, A., Luther, R., Makadia, R., Epifani, E.M., McMahon, J., Merisio, G., Merrill, C.C., Meyer, A.J., Michel, P., Micheli, M., Migliorini, A., Minker, K., Modenini, D., Moreno, F., Murdoch, N., Murphy, B., Naidu, S.P., Nair, H., Nakano, R., Opitom, C., Ormö, J., Owen, J.M., Pajola, M., Palmer, E.E., Palumbo, P., Panicucci, P., Parro, L.M., Pearl, J.M., Penttilä, A., Perna, D., Petrescu, E., Pravec, P., Raducan, S.D., Ramesh, K.T., Ridden-Harper, R., Rizos, J.L., Rossi, A., Roth, N.X., Rożek, A., Rozitis, B., Ryan, E.V., Ryan, W.H., Sánchez, P., Santana-Ros, T., Scheeres, D.J., Scheirich, P., Senel, C.B., Snodgrass, C., Soldini, S., Souami, D., Statler, T.S., Street, R., Stubbs, T.J., Sunshine, J.M., Tan, N.J., Tancredi, G., Tinsman, C.L., Tortora, P., Tusberti, F., Walker, J.D., Waller, C.D., Wünnemann, K., Zannoni, M., Zhang, Y., 2024. Achievement of the planetary defense investigations of the double asteroid redirection test (DART) mission. Planet. Sci. J. 5 (2), 49. http://dx.doi.org/10.3847/PSJ/ad16e6.

Chesley, S.R., French, A.S., Davis, A.B., Jacobson, R.A., Brozović, M., Farnocchia, D., Selznick, S., Liounis, A.J., Hergenrother, C.W., Moreau, M.C., Pelgrift, J., Lessac-Chenen, E., Molaro, J.L., Park, R.S., Rozitis, B., Scheeres, D.J., Takahashi, Y., Vokrouhlický, D., Wolner, C.W.V., Adam, C., Bos, B.J., Christensen, E.J., Emery, J.P., Leonard, J.M., McMahon, J.W., Nolan, M.C., Shelly, F.C., Lauretta, D.S., 2020. Trajectory estimation for particles observed in the vicinity of (101955) Bennu. J. Geophys. Res.: Planets 125 (9), http://dx.doi.org/10.1029/2019JE006363.

Cintala, M.J., Berthoud, L., Hörz, F., 1999. Ejection-velocity distributions from impacts into coarse-grained sand. Meteorit. Planet. Sci. 34 (4), 605–623. http://dx.doi.org/10.1111/j.1945-5100.1999.tb01367.x.

Cintala, M.J., Horz, F., See, T.H., 1989. Impact cratering in low-gravity enviornments: Results of reconnaissance experimentation on the NASA KC-135A reduced gravity aircraft. In: 19th Lunar and Planetary Science Conference. pp. 627–639.

Colwell, J.E., 2003. Low velocity impacts into dust: Results from the COLLIDE-2 microgravity experiment. Icarus 164 (1), 188–196. http://dx.doi.org/10.1016/S0019-1035(03)00083-6.

Colwell, J., Brisset, J., Dove, A., Whizin, A., Nagler, H., Brown, N., Rascon, A., null Brightwell, Seward, L., 2017. Low-velocity impacts into regolith under microgravity conditions. In: Earth and Space 2016. pp. 81–93. http://dx.doi.org/10.1061/9780784479971.010.

Colwell, J.E., Taylor, M., 1999. Low-velocity microgravity impact experiments into simulated regolith. Icarus 138 (2), 241–248. http://dx.doi.org/10.1006/icar.1998.6073.

Daly, R.T., Barnouin, O.S., Bierhaus, E.B., Daly, M.G., Seabrook, J.A., Ballouz, R.L., Nair, H., Espiritu, R.C., Jawin, E.R., Trang, D., et al., 2022. The morphometry of small impact craters on Bennu: Relationships to geologic units, boulders, and impact armoring. Icarus 384, 115058. http://dx.doi.org/10.1016/j.icarus.2022.115058.

Daly, R.T., Bierhaus, E.B., Barnouin, O.S., Daly, M.G., Seabrook, J.A., Roberts, J.H., Ernst, C.M., Perry, M.E., Nair, H., Espiritu, R.C., Palmer, E.E., Gaskell, R.W., Weirich, J.R., Susorney, H.C.M., Johnson, C.L., Walsh, K.J., Nolan, M.C., Jawin, E.R., Michel, P., Trang, D., Lauretta, D.S., 2020. The morphometry of impact craters on Bennu. Geophys. Res. Lett. 47 (24), e2020GL089672. http://dx.doi.org/10.1029/2020GL089672.

Daly, R.T., Ernst, C.M., Barnouin, O.S., Chabot, N.L., Rivkin, A.S., Cheng, A.F., Adams, E.Y., Agrusa, H.F., Abel, E.D., Alford, A.L., et al., 2023. Successful kinetic impact into an asteroid for planetary defence. Nature 616 (7957), 443–447. http://dx.doi.org/10.1038/s41586-023-05810-5.

De Vet, S.J., De Bruyn, J.R., 2007. Shape of impact craters in granular media. Phys. Rev. E - Stat. Nonlinear, Soft Matter Phys. 76 (4), 1–6. http://dx.doi.org/10.1103/PhysRevE.76.041306.

Deboeuf, S., Gondret, P., Rabaud, M., 2009. Dynamics of grain ejection by sphere impact on a granular bed. Phys. Rev. E 79 (4), 1–9. http://dx.doi.org/10.1103/PhysRevE.79.041306.

Dowling, D.R., Dowling, T.R., 2013. Scaling of impact craters in unconsolidated granular materials. Am. J. Phys. 81 (11), 875–878. http://dx.doi.org/10.1119/1.4817309.

Durda, D.D., Chapman, C.R., Merline, W.J., Enke, B.L., 2012. Detecting crater ejecta-blanket boundaries and constraining source crater regions for boulder tracks and elongated secondary craters on Eros. Meteorit. Planet. Sci. 47 (6), 1087–1097.

Gault, D.E., Wedekind, J.A., 1978. Experimental studies of oblique impact. In: Lunar and Planetary Science Conference Proceedings, vol. 9, pp. 3843–3875.

Gautier, F., Sitepu, E., Le Blay, C., Kersey, G., Sánchez, J., 2020. Drop your thesis! 2018 results: 4.74 seconds of microgravity conditions to enable future cubesat landings on asteroids. Acta Astronaut. 176 (November), http://dx.doi.org/10.1016/j.actaastro.2020.06.003.

Hirata, N., Barnouin-Jha, O.S., Honda, C., Nakamura, R., Miyamoto, H., Sasaki, S., Demura, H., Nakamura, A.M., Michikami, T., Gaskell, R.W., et al., 2009. A survey of possible impact structures on 25143 Itokawa. Icarus 200 (2), 486–502. http://dx.doi.org/10.1016/j.icarus.2008.10.027.

Holsapple, K.A., 1993. The scaling of impact processes in planetary sciences. Annu. Rev. Earth Planet. Sci. 21, 333–373.

Holsapple, K.A., Housen, K.R., 2007. A crater and its ejecta: An interpretation of deep impact. Icarus 191, 586–597. http://dx.doi.org/10.1016/j.icarus.2006.08.035.

Holsapple, K., Schmidt, R., 1982. On the scaling of crater dimensions: 2. Impact processes. J. Geophys. Res.: Solid Earth 87 (B3), 1849–1870. http://dx.doi.org/10.1029/JB087iB03p01849.

Housen, K.R., Holsapple, K.A., 2011. Ejecta from impact craters. Icarus 211 (1), 856–875. http://dx.doi.org/10.1016/j.icarus.2010.09.017.

Housen, K., Schmidt, R., Holsapple, K., 1983. Crater ejecta scaling laws: Fundamental forms based on dimensional analysis. J. Geophys. Res.: Solid Earth 88 (B3), 2485–2499. http://dx.doi.org/10.1029/JB088iB03p02485.

Jiang, M.J., Yu, H.S., Harris, D., 2005. A novel discrete model for granular material incorporating rolling resistance. Comput. Geotech. 32, 340–357. http://dx.doi.org/10.1016/j.compgeo.2005.05.001.

Kareta, T., Thomas, C., Li, J.-Y., Knight, M.M., Moskovitz, N., Rożek, A., Bannister, M.T., Ieva, S., Snodgrass, C., Pravec, P., Ryan, E.V., Ryan, W.H., Fahnestock, E.G., Rivkin, A.S., Chabot, N., Fitzsimmons, A., Osip, D., Lister, T., Sarid, G., Hirabayashi, M., Farnham, T., Tancredi, G., Michel, P., Wainscoat, R., Weryk, R., Burrati, B., Pittichová, J., Ridden-Harper, R., Tan, N.J., Tristram, P., Brown, T., Bonavita, M., Burgdorf, M., Khalouei, E., Longa, P., Rabus, M., Sajadian, S., Jorgensen, U.G., Dominik, M., Kikwaya, J.-B., Epifani, E.M., Dotto, E., Deshapriya, P., Hasselmann, P., Dall'Ora, M., Abe, L., Guillot, T., Mékarnia, D., Agabi, A., Bendjoya, P., Suarez, O., Triaud, A., Gasparetto, T., Günther, M.N., Kueppers, M., Merin, B., Chatelain, J., Gomez, E., Usher, H., Stoddard-Jones, C., Bartnik, M., Bellaver, M., Chetan, B., Dugan, E., Fallon, T., Fedewa, J., Gerhard, C., Jacobson, S.A., Painter, S., Peterson, D.-M., Rodriguez, J.E., Smith, C., Sokolovsky, K.V., Sullivan, H., Townley, K., Watson, S., Webb, L., Trigo-Rodríguez, J.M., Llenas, J.M., Pérez-García, I., Castro-Tirado, A.J., Vincent, J.-B., Migliorini, A., Lazzarin, M., Forgia, F.L., Ferrari, F., Polakis, T., Skiff, B., 2023. Ejecta evolution following a planned impact into an asteroid: The first five weeks. Astrophys. J. Lett. 959 (1), L12. http://dx.doi.org/10.3847/2041-8213/ad0fdd.

Katsuragi, H., Blum, J., 2017. The physics of protoplanetesimal dust agglomerates. IX. mechanical properties of dust aggregates probed by a solid-projectile impact. Astrophys. J. 851 (1), 23. http://dx.doi.org/10.3847/1538-4357/aa970d.

Kitazato, K., Milliken, R., Iwata, T., Abe, M., Ohtake, M., Matsuura, S., Arai, T., Nakauchi, Y., Nakamura, T., Matsuoka, M., et al., 2019. The surface composition of asteroid 162173 Ryugu from Hayabusa2 near-infrared spectroscopy. Science 364 (6437), 272–275. http://dx.doi.org/10.1126/science.aav7432.

Kiuchi, M., Nakamura, A.M., Wada, K., 2019. Experimental study on gravitational and atmospheric effects on crater size formed by low-velocity impacts into granular media. J. Geophys. Res.: Planets 124 (5), 1379–1392. http://dx.doi.org/10.1029/2018JE005628.

Kouyama, T., Tatsumi, E., Yokota, Y., Yumoto, K., Yamada, M., Honda, R., Kameda, S., Suzuki, H., Sakatani, N., Hayakawa, M., et al., 2021. Post-arrival calibration of Hayabusa2's optical navigation cameras (ONCs): Severe effects from touchdown events. Icarus 360, 114353. http://dx.doi.org/10.1016/j.icarus.2021.114353.

Kuzmin, R., Shingareva, T., Zabalueva, E., 2003. An engineering model for the Phobos surface. Sol. Syst. Res. 37 (4), 266–281. http://dx.doi.org/10.1023/A:1025074114117.

Langner, K., Marzari, F., Rossi, A., Zanotti, G., 2024. Long-term dynamics around the Didymos–Dimorphos binary asteroid of boulders ejected after the DART impact. Astron. Astrophys. 684, A151. http://dx.doi.org/10.1051/0004-6361/202348675.

Lauretta, D., Hergenrother, C., Chesley, S., Leonard, J., Pelgrift, J., Adam, C., Al Asad, M., Antreasian, P., Ballouz, R.-L., Becker, K., et al., 2019. Episodes of particle ejection from the surface of the active asteroid (101955) Bennu. Science 366 (6470), http://dx.doi.org/10.1126/science.aay3544.

Lauretta, D.S., OSIRIS-REx TAG Team, 2021. The OSIRIS-REx touch-and-go sample acquisition event and implications for the nature of the returned sample. In: Lunar and Planetary Science Conference.

Maurel, C., Michel, P., Biele, J., Ballouz, R.-L., Thuillet, F., 2018. Numerical simulations of the contact between the lander MASCOT and a regolith-covered surface. Adv. Space Res. 62 (8), 2099–2124. http://dx.doi.org/10.1016/j.asr.2017.05.029.

Melosh, H.J., 1989. Impact Cratering: A Geologic Process. Oxford University Press.

Michel, P., Küppers, M., Fitzsimmons, A., Green, S., Lazzarin, M., Ulamec, S., Abell, P., Sugita, S., Campo Bagatin, A., Carry, B., et al., 2025. The Hera space mission in the context of small near-Earth asteroid missions in the past, present and future. Space Sci. Rev. 221 (5), 70. http://dx.doi.org/10.1007/s11214-025-01195-1.

Moreno, F., Tancredi, G., Bagatin, A.C., 2024. On the fate of slow boulders ejected after DART impact on dimorphos. Planet. Sci. J. 5 (3), 63. http://dx.doi.org/10.3847/PSJ/ad26f8.

Murdoch, N., Drilleau, M., Sunday, C., Thuillet, F., Wilhelm, A., Nguyen, G., Gourinat, Y., 2021. Low-velocity impacts into granular material: application to small-body landing. Mon. Not. R. Astron. Soc. http://dx.doi.org/10.1093/mnras/stab624.

Nakamura, A., Michikami, T., Hirata, N., Fujiwara, A., Nakamura, R., Ishiguro, M., Miyamoto, H., Demura, H., Hiraoka, K., Honda, T., et al., 2008. Impact process of boulders on the surface of asteroid 25143 Itokawa—fragments from collisional disruption. Earth, Planets Space 60 (1), 7–12. http://dx.doi.org/10.1186/BF03352756.

Neiderbach, M., Suo, B., Wright, E., Quillen, A., Lee, M., Miklavcic, P., Askari, H., Sánchez, P., 2023. Surface particle motions excited by a low velocity normal impact into a granular medium. Icarus 390, 115301. http://dx.doi.org/10.1016/j.icarus.2022.115301.

Noguchi, R., Hirata, N., Hirata, N., Shimaki, Y., Nishikawa, N., Tanaka, S., Sugiyama, T., Morota, T., Sugita, S., Cho, Y., et al., 2021. Crater depth-to-diameter ratios on asteroid 162173 Ryugu. Icarus 354, 114016. http://dx.doi.org/10.1016/j.icarus.2020.114016.

Pelgrift, J.Y., Lessac-Chenen, E.J., Adam, C.D., Leonard, J.M., Nelson, D.S., McCarthy, L., Sahr, E.M., Liounis, A., Moreau, M., Bos, B.J., Hergenrother, C.W., Lauretta, D.S., 2020. Reconstruction of Bennu particle events from sparse data. Earth Space Sci. 7 (8), e2019EA000938. http://dx.doi.org/10.1029/2019EA000938.

Richardson, D.C., Blum, J., Weinhart, T., Schwartz, S.R., Michel, P., Walsh, K.J., 2012. Numerical simulations of landslides calibrated against laboratory experiments for application to asteroid surface processes. In: AAS/Division for Planetary Sciences Meeting Abstracts #44.

Richardson, J.E., Melosh, H.J., Lisse, C.M., Carcich, B., 2007. A ballistics analysis of the Deep Impact ejecta plume: Determining Comet Tempel 1's gravity, mass, and density. Icarus 191, 176–209. http://dx.doi.org/10.1016/j.icarus.2007.08.033.

Rossi, A., Marzari, F., Brucato, J.R., Della Corte, V., Dotto, E., Ieva, S., Ivanovski, S.L., Lucchetti, A., Epifani, E.M., Pajola, M., et al., 2022. Dynamical evolution of ejecta from the DART impact on Dimorphos. Planet. Sci. J. 3 (5), 118. http://dx.doi.org/10.3847/PSJ/ac686c.

Sakatani, N., Tanaka, S., Okada, T., Fukuhara, T., Riu, L., Sugita, S., Honda, R., Morota, T., Kameda, S., Yokota, Y., et al., 2021. Anomalously porous boulders on (162173) Ryugu as primordial materials from its parent body. Nat. Astron. 5 (8), 766–774. http://dx.doi.org/10.1038/s41550-021-01371-7.

Sánchez, P., Scheeres, D.J., 2011. Simulating asteroid rubble piles with a self-gravitating soft-sphere distinct element method model. Astrophys. J. 727 (2), 120. http://dx.doi.org/10.1088/0004-637X/727/2/120.

Scheeres, D., French, A., Tricarico, P., Chesley, S., Takahashi, Y., Farnocchia, D., McMahon, J., Brack, D., Davis, A., Ballouz, R.-L., et al., 2020a. Heterogeneous mass distribution of the rubble-pile asteroid (101955) Bennu. Sci. Adv. 6 (41), eabc3350. http://dx.doi.org/10.1126/sciadv.abc3350.

Scheeres, D., McMahon, J., Brack, D., French, A., Chesley, S., Farnocchia, D., Vokrouhlickỳ, D., Ballouz, R.-L., Emery, J., Rozitis, B., et al., 2020b. Particle ejection contributions to the rotational acceleration and orbit evolution of asteroid (101955) Bennu. J. Geophys. Res.: Planets 125 (3), e2019JE006284. http://dx.doi.org/10.1029/2019JE006284.

Scheeres, D.J., McMahon, J.W., French, A.S., Brack, D.N., Chesley, S.R., Farnocchia, D., Takahashi, Y., Leonard, J.M., Geeraert, J., Page, B., Antreasian, P., Getzandanner, K., Rowlands, D., Mazarico, E.M., Small, J., Highsmith, D.E., Moreau, M., Emery, J.P., Rozitis, B., Hirabayashi, M., Sánchez, P., Van wal, S., Tricarico, P., Ballouz, R.L., et al., 2019. The dynamic geophysical environment of (101955) Bennu based on OSIRIS-REx measurements. Nat. Astron. 3 (4), 352–361. http://dx.doi.org/10.1038/s41550-019-0721-3.

Schmidt, R.M., Housen, K.R., 1987. Some recent advances in the scaling of impact and explosion cratering. Int. J. Impact Eng. 5 (1–4), 543–560. http://dx.doi.org/10.1016/0734-743X(87)90069-8.

Scholten, F., Preusker, F., Elgner, S., Matz, K.-D., Jaumann, R., Biele, J., Hercik, D., Auster, H.-U., Hamm, M., Grott, M., Grimm, C., Ho, T.-M., Koncz, A., Schmitz, N., Trauthan, F., Kameda, S., Sugita, S., Honda, R., Morota, T., Tatsumi, E., Cho, Y., Yoshioka, K., Sawada, H., Yokota, Y., Sakatani, N., Hayakawa, M., Matsuoka, M., Yamada, M., Kouyama, T., Suzuki, H., Honda, C., Ogawa, K., 2019. The descent and bouncing path of the Hayabusa2 lander MASCOT at asteroid (162173) Ryugu. Astron. Astrophys. 632, L3. http://dx.doi.org/10.1051/0004-6361/201936757.

Schwartz, S.R., Michel, P., Richardson, D.C., Yano, H., 2014. Low-speed impact simulations into regolith in support of asteroid sampling mechanism design I: Comparison with 1-g experiments. Planet. Space Sci. 103, 174–183. http://dx.doi.org/10.1016/j.pss.2014.07.013, arXiv:arXiv:1408.1979v1.

Schwartz, S.R., Richardson, D.C., Michel, P., 2012. An implementation of the soft-sphere discrete element method in a high-performance parallel gravity tree-code. Granul. Matter 14 (3), 363–380. http://dx.doi.org/10.1007/s10035-012-0346-z.

Seguin, A., Bertho, Y., Gondret, P., 2008. Influence of confinement on granular penetration by impact. Phys. Rev. E 78 (1), http://dx.doi.org/10.1103/PhysRevE.78.010301.

Suo, B., Quillen, A., Neiderbach, M., O'Brient, L., Miakhel, A.S., Skerrett, N., Couturier, J., Lherm, V., Wang, J., Askari, H., Wright, E., Sánchez, P., 2024. Subsurface pulse, crater and ejecta asymmetry from oblique impacts into granular media. Icarus 408, 115816. http://dx.doi.org/10.1016/j.icarus.2023.115816.

Takizawa, S., Katsuragi, H., 2020. Scaling laws for the oblique impact cratering on an inclined granular surface. Icarus 335 (113409), http://dx.doi.org/10.1016/j.icarus.2019.113409.

Tancredi, G., Liu, P.-Y., Campo-Bagatin, A., Moreno, F., Domínguez, B., 2022. Lofting of low speed ejecta produced in the DART experiment and production of a dust cloud. Mon. Not. R. Astron. Soc. http://dx.doi.org/10.1093/mnras/stac3258.

Tancredi, G., Maciel, A., Heredia, L., Richeri, P., Nesmachnow, S., 2012. Granular physics in low-gravity environments using discrete element method. Mon. Not. R. Astron. Soc. 420 (4), 3368–3380. http://dx.doi.org/10.1111/j.1365-2966.2011.20259.x.

Thuillet, F., Michel, P., Maurel, C., Ballouz, R.-L., Zhang, Y., Richardson, D.C., Biele, J., Tatsumi, E., Sugita, S., 2018. Numerical modeling of lander interaction with a low-gravity asteroid regolith surface-application to MASCOT on board Hayabusa2. Astron. Astrophys. 615, A41. http://dx.doi.org/10.1051/0004-6361/201832779.

Thuillet, F., Michel, P., Tachibana, S., Ballouz, R.-L., Schwartz, S.R., 2020. Numerical modelling of medium-speed impacts on a granular surface in a low-gravity environment application to Hayabusa2 sampling mechanism. Mon. Not. R. Astron. Soc. 491 (1), 153–177. http://dx.doi.org/10.1093/mnras/stz3010.

Tsuda, Y., Saiki, T., Terui, F., Nakazawa, S., Yoshikawa, M., ichiro Watanabe, S., 2020. Hayabusa2 mission status: Landing, roving and cratering on asteroid Ryugu. Acta Astronaut. 171, 42–54. http://dx.doi.org/10.1016/j.actaastro.2020.02.035.

Tsujido, S., Arakawa, M., Suzuki, A.I., Yasui, M., 2015. Ejecta velocity distribution of impact craters formed on quartz sand: Effect of projectile density on crater scaling law. Icarus 262, 79–92. http://dx.doi.org/10.1016/j.icarus.2015.08.035.

Van wal, S., Çelik, O., Tsuda, Y., Yoshikawa, K., Kawakatsu, Y., 2021. Reduced-gravity experiments of nonspherical rigid-body impact on hard surfaces. Adv. Space Res. 67 (1), 436–476. http://dx.doi.org/10.1016/j.asr.2020.10.018.

Van wal, S., Yoshikawa, K., Tsuda, Y., 2019. Deployment analysis and trajectory reconstruction of minerva-II rovers on asteroid ryugu. In: Advances in the Astronautical Sciences, vol. 168, pp. 1891–1910.

Vance, L.D., Thangavelautham, J., Asphaug, E., Cotto-Figueroa, D., 2022. Possible particle ejection contributions to the shape and spin stability of small near-Earth asteroids. Icarus 115078. http://dx.doi.org/10.1016/j.icarus.2022.115078.

Wada, K., Senshu, H., Matsui, T., 2006. Numerical simulation of impact cratering on granular material. Icarus 180 (2), 528–545. http://dx.doi.org/10.1016/j.icarus.2005.10.002.

Walsh, K.J., Ballouz, R.-L., Jawin, E.R., Avdellidou, C., Barnouin, O.S., Bennett, C.A., Bierhaus, E.B., Bos, B.J., Cambioni, S., Connolly Jr., H.C., et al., 2022. Near-zero cohesion and loose packing of Bennu's near subsurface revealed by spacecraft contact. Sci. Adv. 8 (27), eabm6229. http://dx.doi.org/10.1126/sciadv.abm6229.

Wright, E., Quillen, A.C., South, J., Nelson, R.C., Sanchez, P., Martini, L., Schwartz, S.R., Nakajima, M., Asphaug, E., 2020a. Boulder stranding in ejecta launched by an impact generated seismic pulse. Icarus 337, 113424. http://dx.doi.org/10.1016/j.icarus.2019.113424.

Wright, E., Quillen, A.C., South, J., Nelson, R.C., Sánchez, P., Siu, J., Askari, H., Nakajima, M., Schwartz, S.R., 2020b. Ricochets on asteroids: Experimental study of low velocity grazing impacts into granular media. Icarus 351 (113963), http://dx.doi.org/10.1016/j.icarus.2020.113963.

Yamamoto, S., Wada, K., Okabe, N., Matsui, T., 2006. Transient crater growth in granular targets: An experimental study of low velocity impacts into glass sphere targets. Icarus 183 (1), 215–224. http://dx.doi.org/10.1016/j.icarus.2006.02.002.

Yano, H., Kubota, T., Miyamoto, H., Okada, T., Scheeres, D., Takagi, Y., Yoshida, K., Abe, M., Abe, S., Fujiwara, a., Hasegawa, S., Hashimoto, T., Ishiguro, M., Kato, M., Kawaguchi, J., Mukai, T., Saito, J., Sasaki, S., Yoshikawa, M., 2005. Touchdown of the Hayabusa spacecraft at the Muses Sea on Itokawa. Science 312 (June), 4–7. http://dx.doi.org/10.1126/science.1126164.

Yu, Y., Richardson, D.C., Michel, P., Schwartz, S.R., Ballouz, R.-L., 2014. Numerical predictions of surface effects during the 2029 close approach of Asteroid 99942 Apophis. Icarus 242, 82–96. http://dx.doi.org/10.1016/j.icarus.2014.07.027.

Zhang, Y., Richardson, D.C., Barnouin, O.S., Maurel, C., Michel, P., Schwartz, S.R., Ballouz, R.-L., Benner, L.A., Naidu, S.P., Li, J., 2017. Creep stability of the proposed AIDA mission target 65803 Didymos: I. Discrete cohesionless granular physics model. Icarus 294, 98–123. http://dx.doi.org/10.1016/j.icarus.2017.04.027.